J. Fluid Mech. (2000), *vol.* 408, *pp.* 83–120. Printed in the United Kingdom

© 2000 Cambridge University Press

Subgrid-scale interactions in a numerically simulated planar turbulent jet and implications for modelling

By R. AKHAVAN, A. ANSARI, S. KANG AND N. MANGIAVACCHI

Department of Mechanical Engineering and Applied Mechanics, The University of Michigan, Ann Arbor, MI 48109-2125, USA

(Received 17 February 1999 and in revised form 9 November 1999)

The dynamics of subgrid-scale energy transfer in turbulence is investigated in a database of a planar turbulent jet at $Re_\lambda \approx 110$, obtained by direct numerical simulation. In agreement with analytical predictions (Kraichnan 1976), subgrid-scale energy transfer is found to arise from two effects: one involving non-local interactions between the resolved scales and disparate subgrid scales, the other involving local interactions between the resolved and subgrid scales near the cutoff. The former gives rise to a positive, wavenumber-independent eddy-viscosity distribution in the spectral space, and is manifested as low-intensity, forward transfers of energy in the physical space. The latter gives rise to positive and negative cusps in the spectral eddy-viscosity distribution near the cutoff, and appears as intense and coherent regions of forward and reverse transfer of energy in the physical space. Only a narrow band of subgrid wavenumbers, on the order of a fraction of an octave, make the dominant contributions to the latter. A dynamic two-component subgrid-scale model (DTM), incorporating these effects, is proposed. In this model, the non-local forward transfers of energy are parameterized using an eddy-viscosity term, while the local interactions are modelled using the dynamics of the resolved scales near the cutoff. The model naturally accounts for backscatter and correctly predicts the breakdown of the net transfer into forward and reverse contributions in *a priori* tests. The inclusion of the local-interactions term in DTM significantly reduces the variability of the model coefficient compared to that in pure eddy-viscosity models. This eliminates the need for averaging the model coefficient, making DTM well-suited to computations of complex-geometry flows. The proposed model is evaluated in LES of transitional and turbulent jet and channel flows. The results show DTM provides more accurate predictions of the statistics, structure, and spectra than dynamic eddy-viscosity models and remains robust at marginal LES resolutions.

1. Introduction

Large-eddy simulation (LES) provides a promising approach for the computation of high Reynolds number turbulent flows in complex engineering environments, where simpler modelling strategies may be inadequate and the high Reynolds number of the flow prohibits the use of direct numerical simulation (DNS). General reviews are given in Rogallo & Moin (1984), Lesieur & Metais (1996) and the volumes edited by Galperin & Orszag (1993) and Metais & Ferziger (1997).

https://doi.org/10.1017/S0022112099007582 Published online by Cambridge University Press

For incompressible flow, the LES governing equations are given by the filtered Navier–Stokes and continuity equations

$$\frac{\partial \overline{u}_i}{\partial t} + \frac{\partial}{\partial x_j}(\overline{u}_i \overline{u}_j) = -\frac{1}{\rho}\frac{\partial \overline{p}}{\partial x_i} - \frac{\partial \eta_{ij}}{\partial x_j} + \nu \frac{\partial^2 \overline{u}_i}{\partial x_j \partial x_j}, \tag{1.1}$$

$$\frac{\partial \overline{u}_i}{\partial x_i} = 0, \tag{1.2}$$

where

$$\overline{u}_i(\boldsymbol{x}, t) = \int u_i(\boldsymbol{x}, t)\overline{G}(\boldsymbol{x}, \boldsymbol{x}')\,\mathrm{d}\boldsymbol{x}' \tag{1.3}$$

is the resolved velocity field and $\overline{G}(\boldsymbol{x}, \boldsymbol{x}')$ is a spatial filter of characteristic width $\overline{\Delta}_i$ in the ith-direction. The effect of the subgrid scales (SGS) on the resolved flow is captured in the turbulent stress

$$\eta_{ij} = \overline{u_i u_j} - \overline{u}_i \overline{u}_j, \tag{1.4}$$

which is unknown and must be parameterized in terms of the resolved velocity field to close the set of equations (1.1) and (1.2). Alternatively, as shown by Leonard (1974) and Germano (1986), the turbulent stress η_{ij} can be decomposed into a resolvable 'Leonard stress', $L_{ij} = \overline{\overline{u}_i \overline{u}_j} - \overline{u}_i \overline{u}_j$, and a true subgrid-scale stress, $\tau_{ij} = \eta_{ij} - L_{ij}$, and the modelling applied only to τ_{ij}. For sharp (cutoff/Fourier) filters, $\tau_{ij} = \overline{u_i u_j} - \overline{u}_i \overline{u}_j$ and equation (1.1) can be written as

$$\frac{\partial \overline{u}_i}{\partial t} + \frac{\partial}{\partial x_j}(\overline{\overline{u}_i \overline{u}_j}) = -\frac{1}{\rho}\frac{\partial \overline{p}}{\partial x_i} - \frac{\partial \tau_{ij}}{\partial x_j} + \nu \frac{\partial^2 \overline{u}_i}{\partial x_j \partial x_j}. \tag{1.5}$$

Most existing SGS models are of the eddy-viscosity type and assume a linear gradient transport hypothesis to model the turbulent stress as

$$\eta^*_{ij} = -2\nu_t \overline{S}_{ij}, \tag{1.6}$$

where $\overline{S}_{ij} = \frac{1}{2}(\partial \overline{u}_i/\partial x_j + \partial \overline{u}_j/\partial x_i)$ is the resolved deformation tensor, ν_t is the eddy viscosity, and $\eta^*_{ij} = \eta_{ij} - \frac{1}{3}\delta_{ij}\eta_{kk}$ denotes the deviatoric part of the stress tensor. In the most commonly used eddy-viscosity model, developed by Smagorinsky (1963), the eddy viscosity is parameterized in terms of the magnitude of the resolved deformation tensor and the effective filter width according to

$$\nu_t = (C_S \overline{\Delta})^2 |\overline{S}|, \tag{1.7}$$

where $|\overline{S}| = (2\overline{S}_{ij}\overline{S}_{ij})^{1/2}$ and C_S is a model coefficient. Alternative formulations parameterize ν_t in terms of the resolved vorticity field (Kwak, Reynolds & Ferziger 1975), the subgrid-scale turbulence kinetic energy (Schumann 1975), or the local second-order structure function of the resolved velocity field (Metais & Lesieur 1992).

Eddy-viscosity models are generally constructed to account for the net subgrid-scale dissipation only in a mean or volume-averaged sense. As such, they represent a parameterization of the average eddy viscosity in the resolved scales, not the local and instantaneous ν_t (Lilly 1967; Leslie & Quarini 1979). Many problems arise when the average nature of such parameterizations is ignored and the models are applied to the local eddy-viscosity. In particular, at a local level, eddy-viscosity models show little correlation with the actual subgrid-scale stresses in *a priori* tests (Clark, Ferziger & Reynolds 1979; Bardina, Ferziger & Reynolds 1980; Horiuti 1989; Domaradzki, Liu & Brachet 1993; Domaradzki *et al.* 1994; Liu, Meneveau & Katz 1994). This

https://doi.org/10.1017/S0022112099007582 Published online by Cambridge University Press

is primarily due to the inherently dissipative nature of these models, which make them ill-suited to the representation of the local reverse transfers (backscatter) of energy from the subgrid to the resolved scales of motion. This local backscatter is an important feature of subgrid-scale energy transfer, and can be quite significant (Leslie & Quarini 1979; Piomelli *et al.* 1991; Domaradzki *et al.* 1993, 1994). Recent dynamic formulations of eddy-viscosity parameterizations (Germano *et al.* 1991; Lilly 1992; Ghosal *et al.* 1995; Piomelli & Liu 1995; Meneveau, Lund & Cabot 1996), while making the models more robust, have not resolved either of these problems. In essence, what all these dynamic formulations have re-confirmed is that eddy-viscosity parameterizations are applicable only in an average sense, always requiring some sort of averaging on the model coefficient in order to retain the dissipative nature of the model and avoid numerical instability. Local backscatter is either ignored in dynamic formulations or is introduced through an additional stochastic force in the LES equations (Bertoglio 1985; Chasnov 1991; Leith 1990; Mason & Thomson 1992; Schumann 1995; Carati, Ghosal & Moin 1995). However, such a representation of backscatter, as a random force uncorrelated from one time-step to the next, is not consistent with the known physics of backscatter and has been shown to make little difference in the predicted statistics in LES computations (Carati *et al.* 1995). Despite these limitations, eddy-viscosity models can provide fairly accurate predictions of the mean flow statistics in LES due to their ability to properly account for the net SGS dissipation. Their main drawback lies in their high resolution requirements and difficulty in capturing the structure of the flow.

Similarity models provide an alternative class of SGS parameterizations. Pioneered by Bardina *et al.* (1980) for application with graded filters, these models utilize the high correlations observed between the actual SGS stresses and the stresses arising from the smallest of the resolved scales to approximate the SGS stress tensor in terms of the stresses arising from the resolved scales. In the similarity model of Bardina *et al.* (1980) the SGS stress is modelled as

$$\eta_{ij} \approx \overline{\overline{u}_i \overline{u}_j} - \overline{\overline{u}}_i \overline{\overline{u}}_j, \tag{1.8}$$

which is equivalent to approximating η_{ij} by L_{ij}. A number of generalizations of this parameterization have been proposed in recent years (Liu *et al.* 1994; Salvetti & Banerjee 1995; Shah & Ferziger 1995; Domaradzki & Saiki 1997). These can be broadly represented as

$$\eta_{ij} \approx C_L(\widetilde{\overline{u}_i^* \overline{u}_j^*} - \widetilde{\overline{u}_i^*}\,\widetilde{\overline{u}_j^*}), \tag{1.9}$$

where C_L is a model coefficient, tilde denotes a filter either identical to the LES filter or one similar in shape but of larger width (typically of scale 2Δ), and $\overline{u}_i^*$ is either identical to $\overline{u}_i$ or denotes a higher-order approximation or estimation of $\overline{u}_i$. Similarity models naturally account for backscatter and give high correlations with the actual SGS stresses in *a priori* tests. Their main shortcoming is that they are generally not adequately dissipative. This problem can be alleviated by using extensions of the resolved velocity field in the similarity expression (Shah & Ferziger 1995; Domaradzki & Saiki 1997) or by combining the similarity model with an eddy-viscosity term. A number of such mixed models have been proposed in recent years (Bardina *et al.* 1980; Zang, Street & Koseff 1993; Salvetti & Banerjee 1995; Horiuti 1993, 1997). In LES applications, mixed models perform comparably with or better than pure eddy-viscosity models. However, because the improvements are not dramatic and the results depend on the type of filter used, mixed models have so far gained only limited popularity.

https://doi.org/10.1017/S0022112099007582 Published online by Cambridge University Press

The limitations of existing SGS models suggest that a better understanding of the physics of SGS energy transfer and of the phenomenon of backscatter, in particular, is needed before more faithful SGS parameterizations can be developed. Improved models could potentially lead to a relaxation of the stringent resolution requirements of LES and provide LES with the capability to make structural, in addition to statistical, predictions of the large-scale motions. The energy exchanges between the resolved and subgrid scales of motion can be studied using analytical theories of turbulence (Kraichnan 1976, Leslie & Quarini 1979, Chollet & Lesieur 1981, Lesieur 1991, Zhou & Vahala 1993), direct numerical simulations (Clark *et al.* 1979, Bardina *et al.* 1980, Piomelli *et al.* 1991, Meneveau 1991, Domaradzki *et al.* 1987, 1990, 1993, 1994, Ohkitani & Kida 1992, Piomelli *et al.* 1996), or experiments (Liu *et al.* 1994, O'Neil & Meneveau 1997). These studies have revealed many important characteristics of SGS energy transfer. However, the implementation of these ideas into SGS models has been limited.

The objective of the present study is to provide a better understanding of the dynamics of SGS energy transfer in turbulent shear flows and to incorporate this understanding into improved SGS models for LES of turbulence in engineering applications. The studies are based on an analysis of a database of a temporally-growing planar turbulent jet at $Re_\lambda \approx 110$, obtained by direct numerical simulation (DNS). The organization of the paper is as follows. In § 2 the numerical database of the turbulent jet and the methods of data analysis are briefly reviewed. The dynamics of SGS energy transfer in the spectral space and physical space are discussed in § 3 and § 4. In § 5 a subgrid-scale parameterization incorporating these dynamics is proposed. The performance of the proposed model is evaluated by *a priori* tests in § 6 and by LES of transitional and turbulent flows in § 7. The extension of the model to graded filters is discussed in § 8. Conclusions and a summary are given in § 9.

2. Numerical database and data analysis

2.1. *The DNS database of the jet*

Jet flow was chosen as a prototype turbulent shear flow in the study of subgrid-scale interactions because of its simplicity and the relatively high Reynolds numbers which can be attained in this flow by DNS. Various details of the simulation as well as a discussion of the evolution, statistics and structure of the jet is given in Ansari (1993). Here we briefly summarize the main features of the flow which are relevant to the present discussion.

The jet is assumed to be periodic in the streamwise (x) and spanwise (y) directions and infinite in extent in the lateral (z) direction. The simulations were performed with a resolution of $128\times128\times256$ de-aliased modes using standard pseudo-spectral methods, and employed Fourier series in the homogeneous directions and mapped Chebyshev polynomials in the lateral direction. The computations were started from a laminar jet with a blunt (hyperbolic-tangent) velocity profile with characteristic centreline velocity U_0 and jet half-width z_0, on which an infinitesimal random noise disturbance field was superimposed. The jet undergoes transition to turbulence between the times of $30 < tU_0/z_0 < 70$ and equilibrates to a stationary turbulent state with self-preserving velocity profiles thereafter. The subgrid-scale interactions reported in this paper are from the time $tU_0/z_0 = 100$. At this time, the jet had a turbulent Reynolds number of $Re_\lambda \approx 110$ based on the lateral Taylor microscale, and a corresponding bulk Reynolds number of $Re_b = U_c\delta/\nu = 6800$ based on the jet centreline velocity and full jet width.

https://doi.org/10.1017/S0022112099007582 Published online by Cambridge University Press

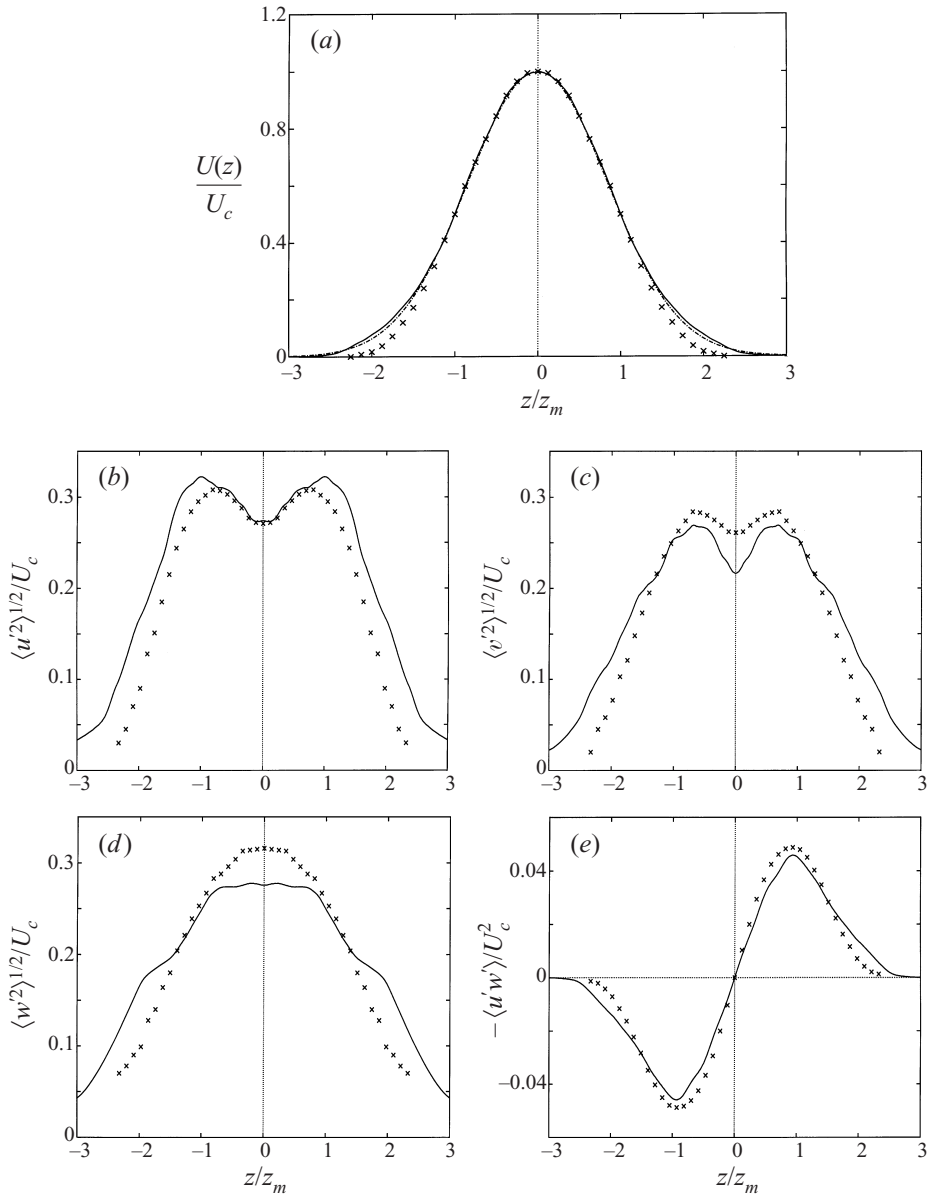


FIGURE 1. Mean turbulence statistics in the fully developed turbulent temporally growing planar jet compared to experimental measurements in spatially growing turbulent planar wakes: ——, DNS; ×, wake data of Townsend (1949); — · — · —, Gaussian curve (2.1).

The effective grid spacing at this time was on the order of 4 Kolmogorov scales in the homogeneous (x and y) directions and 2 Kolmogorov scales in the lateral direction.

Figure 1 shows the mean turbulence statistics in the jet at $tU_0/z_0 = 100$. The mean velocity profile is in agreement with the Gaussian distribution

$$\frac{U(z,t)}{U_c(t)} = \mathrm{e}^{-0.693(z/z_m)^2}, \tag{2.1}$$

which represents the analytical mean velocity profile in a self-preserving temporally

https://doi.org/10.1017/S0022112099007582 Published online by Cambridge University Press

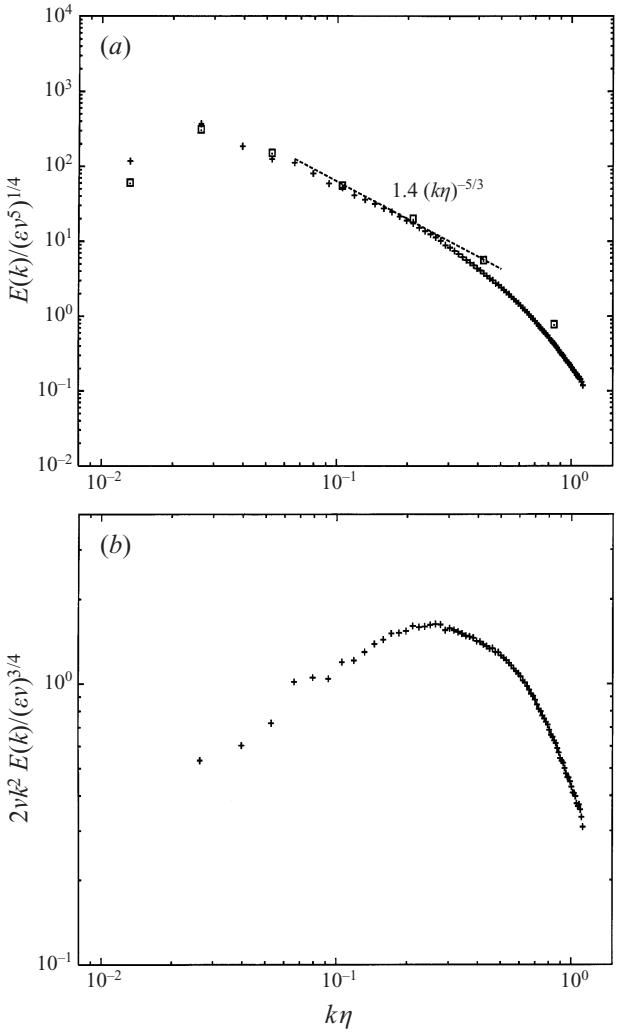


FIGURE 2. Three-dimensional spectra of (*a*) kinetic energy, and (*b*) kinetic energy dissipation in the jet obtained using the Fourier and wavelet representations: +, Fourier; □, wavelet.

growing planar turbulent jet with a constant eddy viscosity. The statistics are also in reasonably good agreement with experimental measurements in spatially growing planar turbulent far wakes (Townsend 1949), whose evolution and governing equations are analogous to the temporally growing jet.

The three-dimensional kinetic energy and dissipation spectra in the jet at $tU_0/z_0 = 100$ are shown in figures 2(*a*) and 2(*b*). The spectra were computed by truncating the domain in the lateral direction to $-3.2 < z/z_m < 3.2$, interpolating the data onto a uniform Fourier grid using spectral interpolation, and computing the spectra using the conventional definitions. The spectra are normalized using the average rate of kinetic energy dissipation, ε, in the truncated jet and the corresponding Kolmogorov scale, $\eta = (\nu^3/\varepsilon)^{1/4}$. Over the range of wavenumbers $0.07 < k\eta < 0.2$ the energy spectrum conforms to the inertial $k^{-5/3}$ law with a Kolmogorov constant of $C_K = 1.4$, which is in good agreement with the value $C_K \approx 1.5$ observed in experimental studies (Monin & Yaglom 1981). The dissipation spectrum attains its peak at $k\eta \approx 0.2$, in

https://doi.org/10.1017/S0022112099007582 Published online by Cambridge University Press

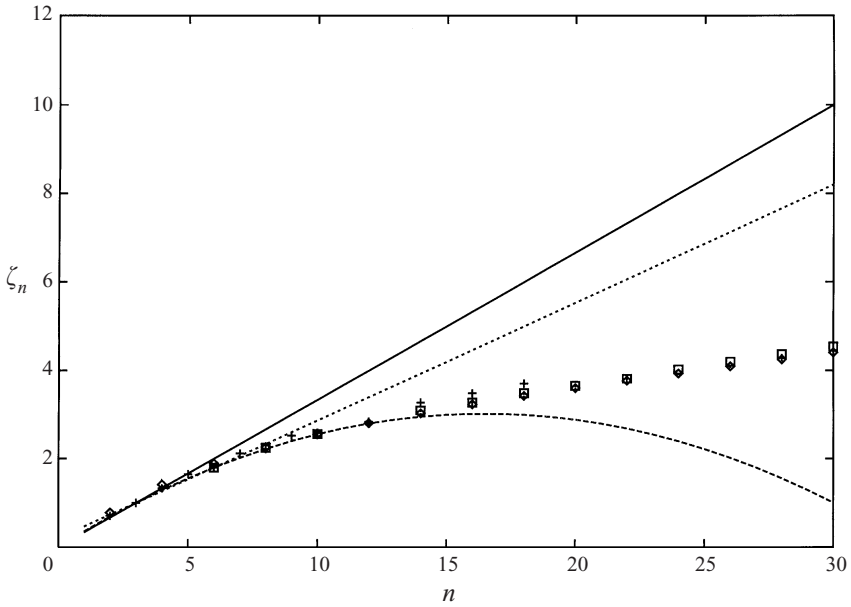


FIGURE 3. Scaling exponents of the velocity structure functions, ζ_n, for even n: ◇, DNS of planar turbulent jet; □, DNS of isotropic turbulence by Vincent *et al.* (1991); +, measurements in a round jet at $Re_\lambda = 852$ by Anselmet *et al.* (1984); ——, Kolmogorov (1941) theory; - - -, Kolmogorov (1961) theory; · · · · · ·, β-model.

agreement with the results obtained in other numerical simulations of turbulence (e.g. Kida & Murakami 1987; Domaradzki 1992) and the wavenumber of peak dissipation predicted by Pao's (1965) spectrum with a Kolmogorov constant of 1.4.

The inertial-range properties of the jet flow were further characterized by examining the scaling exponents of the longitudinal velocity structure functions, ζ_n, defined as $\langle|\Delta u'(r_x)|^n\rangle_V = K_n(\langle\epsilon\rangle_V r_x)^{\zeta_n}$, where $\langle|\Delta u'(r_x)|^n\rangle_V = \langle|u'(\boldsymbol{x}+r_x)-u'(\boldsymbol{x})|^n\rangle_V$ and r_x is a longitudinal separation in the inertial range. The scaling exponents were computed using the so-called 'direct method' (Anslemet *et al.* 1984), from the slopes of linear regression best fits to logarithmic plots of $\langle|\Delta u'(r_x)|^n\rangle_V$ plotted as a function of r_x for r_x in the inertial range ($15 < r_x/\eta < 45$). Figure 3 shows the scaling exponents for even-ordered moments of the longitudinal velocity differences in the jet. Also shown are the scaling exponents reported by Anselmet *et al.* (1984) in an axisymmetric jet at $Re_\lambda \approx 850$, by Vincent & Meneguzzi (1991) in a numerical database of homogeneous turbulence at $Re_\lambda \approx 150$, and a number of classical models: Kolmogorov's (1941) model ($\zeta_n = n/3$), Kolmogorov's (1961) log-normal model ($\zeta_n = 1/3n - 1/18\mu n(n-3)$, with $\mu = 0.2$) and the β-model of Frisch, Sulem & Nelkin (1978) ($\zeta_n = 1/3n - 1/3\mu(n-3)$). The agreement between the scaling exponents in the present jet flow and measurements in higher Reynolds number flows gives us confidence that, despite the relatively short inertial range of the present database, the observed dynamics is representative of higher Reynolds number flows for which subgrid-scale models are intended.

2.2. *Data analysis*

Subgrid-scale interactions were studied using a combination of Fourier and wavelet methods. Fourier analysis is the traditional tool for investigating the spectral dynamics

https://doi.org/10.1017/S0022112099007582 Published online by Cambridge University Press

of turbulence and, as such, allows comparisons with many known analytical results. The main limitation of a Fourier analysis is that the spectral information it supplies represents the average over the flow domain and does not contain information on the spatial variability of various spectral distributions. This information is readily available in a wavelet representation. Because of this and other desirable properties, wavelets have found extensive application in the analysis, modelling, and computation of turbulence in recent years (e.g. Farge 1992; Farge *et al.* 1996, and references therein). In this study, the wavelet analysis is used primarily to investigate the breakdown of the spectral eddy viscosity into forward and reverse transfers and to characterize the nonlinear interactions which contribute to these transfers. While it is possible to obtain this information using Fourier methods (Domaradzki *et al.* 1993), such an analysis requires examining the individual triad interactions and has not been attempted here.

Our methodology for the wavelet analysis is similar to that proposed by Mallat (1989) and Meneveau (1991). Here we only briefly summarize the features relevant to the present discussion. In the wavelet representation, flow quantities such as the disturbance velocity $u'_\alpha(\boldsymbol{x})$ are expressed in terms of discrete orthonormal wavelet basis functions (Daubechies 1988; Mallat 1989; Meneveau 1991)

$$u'_\alpha(\boldsymbol{x}) = \sum_{q=1}^{7} \sum_{n=1}^{N} \sum_{\boldsymbol{i}} u'^{(n,q)}_\alpha[\boldsymbol{i}]\, \Psi^{(n,q)}(\boldsymbol{x} - 2^n h\boldsymbol{i}), \tag{2.2}$$

where n denotes the scale measured in octave bands, $\boldsymbol{i}$ is the three-dimensional position index in a box of mesh size $2^n h$, and h denotes the mesh size at the smallest scale. The summation over the index q arises from the method used to construct the three-dimensional wavelet basis functions $\Psi^{(n,q)}(\boldsymbol{x} - 2^n h\boldsymbol{i})$ in terms of products of one-dimensional wavelets along the three Cartesian directions. We use the 8-point orthonormal wavelets with compact support suggested by Daubechies (1988) for these one-dimensional wavelets.

Using the wavelet representation, various spectral flow quantities can be computed while retaining information on their spatial distributions. For example, the local kinetic energy at scale n and location $2^n h\boldsymbol{i}$ can be computed as

$$e^{(n)}[\boldsymbol{i}] = \frac{1}{2} \sum_{q=1}^{7} u'^{(n,q)}_\alpha u'^{(n,q)}_\alpha. \tag{2.3}$$

Quantities such as this can be examined directly in the mixed spectral/physical representation or converted to traditional spectral quantities. For instance, one can use (2.3) to compute the energy spectrum as

$$E_w(k) = \frac{\sum_{\boldsymbol{i}} e^{(n)}[\boldsymbol{i}]}{2^{3N} k \ln(2)}, \tag{2.4}$$

where $k = 2\pi/2^n h$ is the effective wavenumber, $\Delta k = k \ln(2)$ is the effective bandwidth, and 2^{3N} is the total number of points in the domain. Figure 2(a) shows the comparison between the kinetic energy spectra computed by the wavelet and Fourier methods. The two spectra are in good general agreement, verifying the accuracy of the wavelet analysis. The small differences between the two spectra observed at high wavenumbers reflects the different bandwidths over which the spectral energy density is computed in the two representations.

https://doi.org/10.1017/S0022112099007582 Published online by Cambridge University Press

3. Subgrid-scale interactions in the spectral space

To study the subgrid-scale interactions, a sharp (Fourier) filter is employed to divide the wavenumber space into two regions: $\mathscr{L}$ corresponding to $|\boldsymbol{k}| \leqslant k_m$ and denoting the large or resolved scales, and $\mathscr{S}$ corresponding to $|\boldsymbol{k}| > k_m$ and denoting the small or subgrid scales. The dynamics of subgrid-scale energy transfer in the spectral space can be most conveniently analysed by examining the characteristics of the spectral eddy viscosity, $\nu(k|k_m)$, as introduced by Kraichnan (1976). In the Fourier representation, the spectral eddy viscosity is given by

$$\nu(k|k_m) = -\frac{T_S(k|k_m)}{2k^2E(k)}, \qquad k \leqslant k_m, \tag{3.1}$$

where $T_S(k|k_m)$ represents the transfer of energy to a resolved scale k due to nonlinear interactions with scales larger than k_m (see Appendix A). The analogous quantity in the wavelet representation is the spectral eddy viscosity acting on a resolved scale n at location $2^n h\boldsymbol{i}$ due to dynamical interactions with scales larger than m. This can be defined as

$$\nu^{(n|m)}[\boldsymbol{i}] = -\frac{t_s^{(n|m)}[\boldsymbol{i}]}{d^{(n)}[\boldsymbol{i}]}, \tag{3.2}$$

where $t_s^{(n|m)}[\boldsymbol{i}]$ denotes the subgrid-scale transfer of energy to scale n at location $2^n h\boldsymbol{i}$ and $d^{(n)}[\boldsymbol{i}] = \sum_{q=1}^{7} u'^{(n,q)}_{\alpha}[\boldsymbol{i}]\{-\nabla^2 u'_{\alpha}\}^{(n,q)}[\boldsymbol{i}]$. The average of $\nu^{(n|m)}[\boldsymbol{i}]$ over all physical locations is the wavelet equivalent of the spectral eddy viscosity

$$\nu_w(k|k_m) = \frac{1}{2^{3(N-n)}} \sum_{\boldsymbol{i}} \nu^{(n|m)}[\boldsymbol{i}], \tag{3.3}$$

where $k = 2\pi/2^n h$ and $k_m = 2\pi/2^m h$. The wavelet representation also provides information on the breakdown of $\nu(k|k_m)$ into forward, $\nu_w^+(k|k_m)$, and reverse, $\nu_w^-(k|k_m)$, contributions:

$$\nu_w^+(k|k_m) = \frac{1}{2^{3(N-n)}} \sum_{\boldsymbol{i}} \nu^{(n|m)}[\boldsymbol{i}], \qquad \nu^{(n|m)} > 0; \tag{3.4}$$

$$\nu_w^-(k|k_m) = \frac{1}{2^{3(N-n)}} \sum_{\boldsymbol{i}} \nu^{(n|m)}[\boldsymbol{i}], \qquad \nu^{(n|m)} < 0. \tag{3.5}$$

Figure 4 shows the distributions of $\nu(k|k_m)$ in the jet obtained using the Fourier and wavelet methods for two values of the cutoff wavenumber: $k_m\eta = 0.18$ in the inertial range, and $k_m\eta = 0.39$ in the dissipation range. Also shown are the breakdown of $\nu_w(k|k_m)$ into $\nu_w^+(k|k_m)$ and $\nu_w^-(k|k_m)$, and the analytical prediction of $\nu(k|k_m)$ by Kraichnan (1976) based on the test-field model assuming isotropic turbulence with an infinitely long inertial-range spectrum and a Kolmogorov constant of 1.4. A similar analytical distribution is also predicted by the eddy-damped quasi-normal Markovian (EDQNM) theory (Chollet & Lesieur 1981; Lesieur 1991). The Fourier and wavelet results are in close agreement with each other and with the analytical prediction of Kraichnan (1976). As before, an exact agreement between the Fourier and wavelet results cannot be expected since the latter represents the average of $\nu(k|k_m)$ over a wider band of wavenumbers than the former. One consequence of this is that the cusps in the curve of $\nu(k|k_m)$ become less pronounced in the wavelet representation. The spectral eddy viscosity in the jet also agrees qualitatively with earlier results reported in numerical databases of isotropic turbulence (Domaradzki *et al.* 1987, 1993; Lesieur 1991; Meneveau 1991). The main difference between the present results

https://doi.org/10.1017/S0022112099007582 Published online by Cambridge University Press

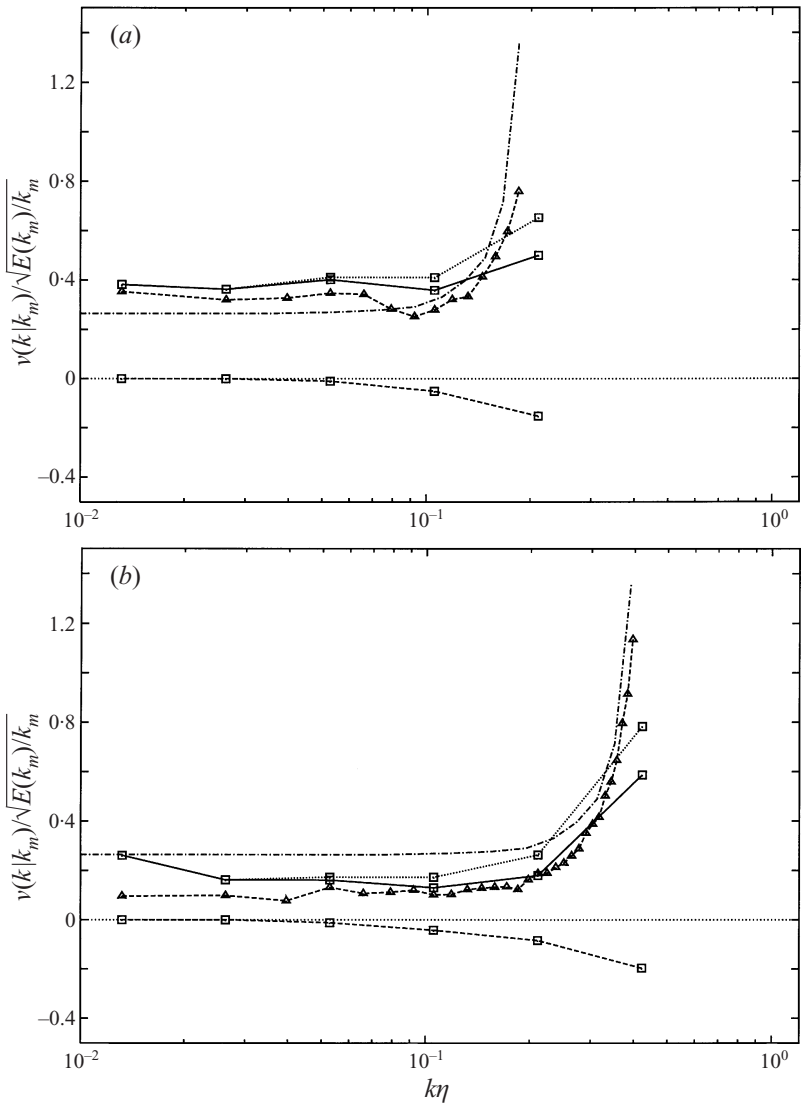


FIGURE 4. The spectral eddy viscosity, $\nu(k|k_m)$, acting on a scale k due to dynamical interactions with scales larger than k_m computed using the Fourier and wavelet representations for (*a*) $k_m\eta = 0.18$ (in the inertial range), and (*b*) $k_m\eta = 0.39$ (in the dissipation range). Also shown are the breakdown of $\nu_w(k|k_m)$ into forward and reverse contributions. – –△– –, $\nu(k|k_m)$ from Fourier analysis; –□–, $\nu_w(k|k_m)$; · ·⊡· ·, $\nu_w^+(k|k_m)$; – –□– –, $\nu_w^-(k|k_m)$; – · – · –, analytical prediction of $\nu(k|k_m)$ from Kraichnan (1976).

and those reported earlier is in the value of the low-wavenumber asymptote of the spectral eddy viscosity. In the present results, this asymptote has a finite value, in agreement with analytical predictions, whereas earlier studies showed a near-zero asymptote, reflecting the absence of a true inertial range in the databases used in those studies.

A number of important dynamical features of subgrid-scale energy transfer are displayed in the characteristics of $\nu(k|k_m)$, as noted by Kraichnan (1976) and others (Leslie & Quarini 1979; Chollet & Lesieur 1981). In particular, the eddy viscosity

https://doi.org/10.1017/S0022112099007582 Published online by Cambridge University Press

exhibits a dual character. For $k \ll k_m$, the spectral eddy viscosity asymptotes to a constant value and is primarily composed of low-intensity forward transfers of energy. By construction, these transfers represent non-local energy transfers between a resolved mode $k \ll k_m$ and two subgrid modes $p \gg k$ and $q \gg k$. The presence of a large separation of scales, combined with the asymptotic and positive nature of the spectral eddy viscosity in this regime, suggests that an eddy viscosity model should be able to accurately represent this portion of the subgrid-scale interactions. A different behaviour is observed near the cutoff. Here $\nu(k|k_m)$ rises sharply to a cusp and is composed of both positive and negative contributions. The dominant dynamical interactions at work here are local triadic interactions between a resolved mode $k \sim k_m$ and subgrid modes $p \sim q \sim k_m$. These interactions represent local transfers of energy and, therefore, cannot be faithfully represented by an eddy-viscosity model. The cusps are not an intrinsic feature of turbulence, but a manifestation of the absence of the modes $k > k_m$ in the dynamics of the resolved scales. If the additional modes were present, so that the triadic interactions could be summed over all possible triads, the cusps would disappear and the spectral eddy viscosity would revert to that observed at low wavenumbers. Therefore, the intensity of the cusps is strongly dependent upon the characteristics of the filter used.

For modelling, it is important to establish which range of subgrid wavenumbers contributes to these local interactions. This can be determined by examining the subgrid-scale energy transfer in truncated databases of the velocity field, obtained from the original field by setting all modes with a wavenumber greater than a prescribed value k_t equal to zero. The subgrid-scale energy transfer in these truncated databases would then represent the interactions between the resolved modes $|\boldsymbol{k}| \leqslant k_m$ and only the range of subgrid modes $k_m < |\boldsymbol{k}| \leqslant k_t$. Figure 5 shows $\nu_w(k|k_m;k_t)$ in the jet for $k_m\eta = 0.18$ and three values of $k_t/k_m = 2.0$, 1.5, and 1.25. Also shown are $\nu_w(k|k_m)$ in the original (non-truncated) field, and the breakdown of each into positive (ν_w^+) and negative (ν_w^-) contributions. For all values of $1.25 < k_t/k_m < 2.0$, eliminating all subgrid modes with a wavenumber greater than k_t affects only the non-local forward transfers of energy, resulting in a uniform downward shift of the curves of ν_w and ν_w^+ from their original values. However, the cusps in the curves of ν_w and ν_w^+ and the entire curve of ν_w^- remain unaffected. This establishes the degree of locality of the interactions which contribute to the cusps, and shows that the predominant contributions arise from only a very narrow band of subgrid wavenumbers corresponding to $k_m < k < 1.25k_m$, not the whole range $k_m < k < 2k_m$ as suggested in the past (Domaradzki & Saiki 1997). This opens up new possibilities for modelling these local interactions, as discussed in § 5.

Another issue is the relative importance of the local and non-local interactions in the overall dynamics of transfer. This can be established by examining the quantity (Kraichnan 1976)

$$\Pi_{sg}(k|k_m) = \frac{\displaystyle\int_k^{k_m} T_S(k'|k_m)\,\mathrm{d}k'}{\displaystyle\int_0^{k_m} T_S(k'|k_m)\,\mathrm{d}k'}, \tag{3.6}$$

which represents the fraction of subgrid-scale energy transfer arising from interactions between the resolved scales $k < k' < k_m$ and the entire subgrid scales. Figure 6 shows $\Pi_{sg}(k|k_m)$ in the jet for the two cutoff wavenumbers $k_m\eta = 0.18$ and $k_m\eta = 0.39$. In each case, more than half of the net transfer arises from interactions between the subgrid scales and the highest 25% of the resolved modes ($0.75 < k/k_m < 1.0$),

https://doi.org/10.1017/S0022112099007582 Published online by Cambridge University Press

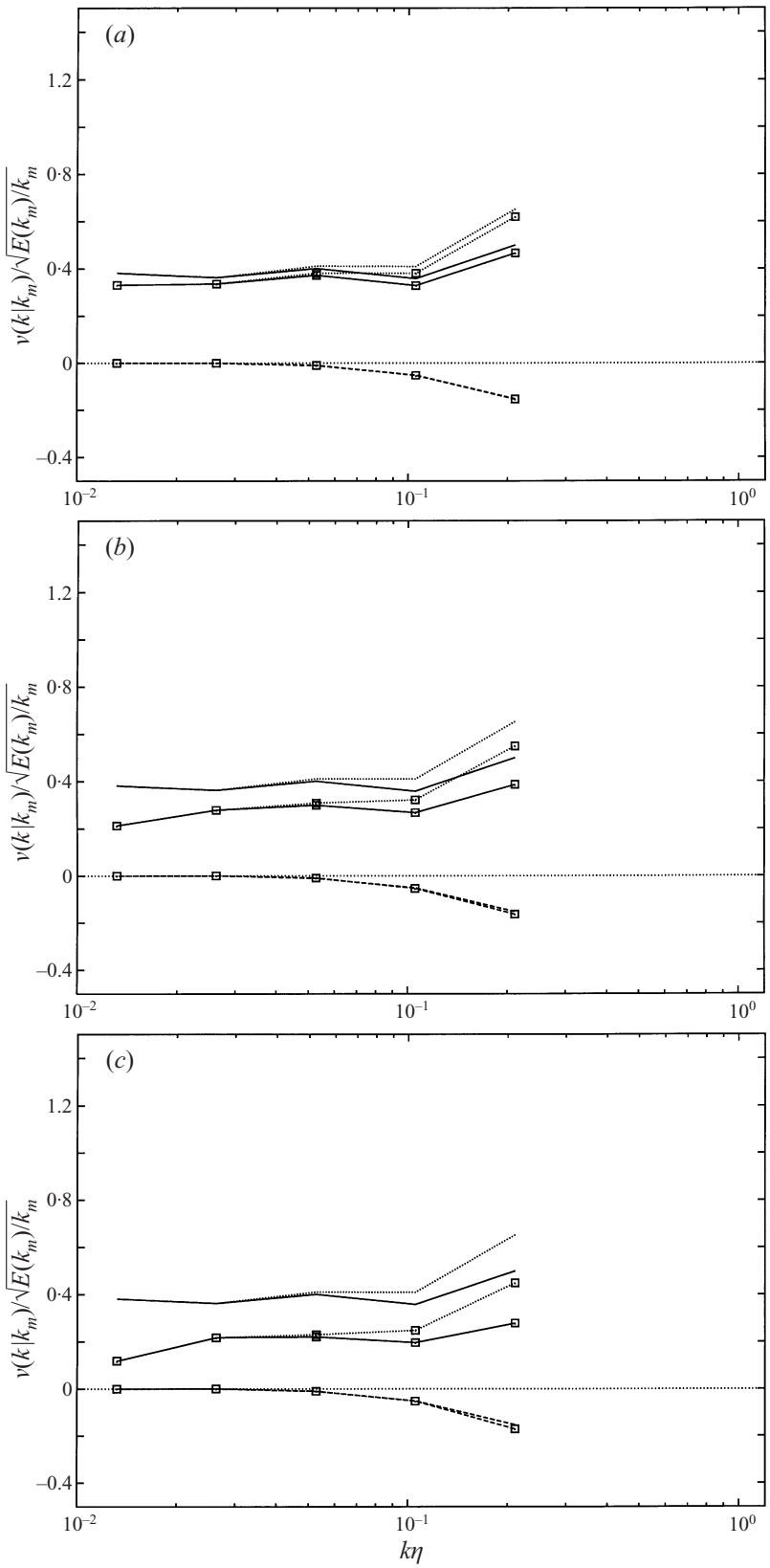


FIGURE 5. For caption see facing page.

https://doi.org/10.1017/S0022112099007582 Published online by Cambridge University Press

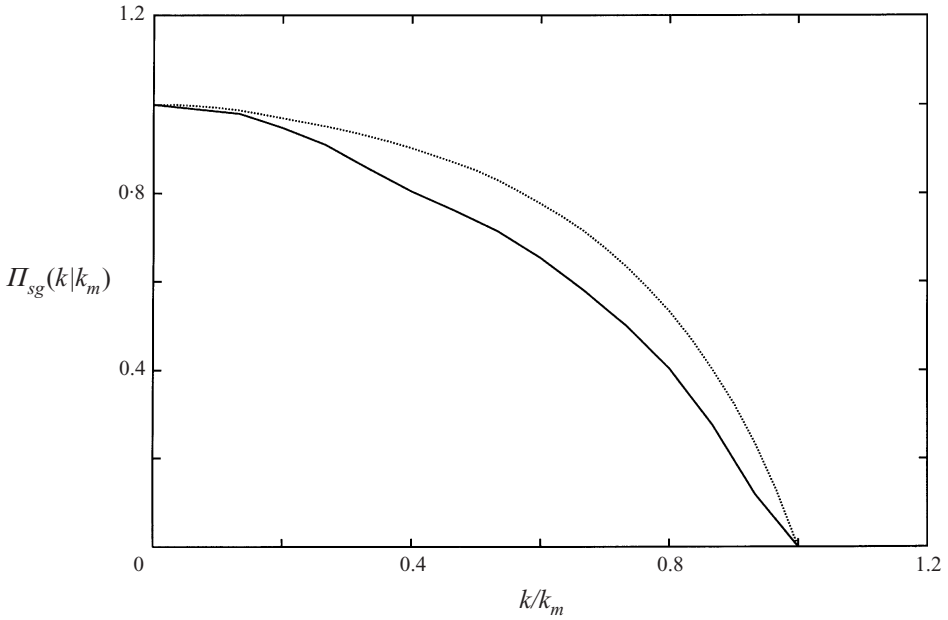


FIGURE 6. The fraction of subgrid-scale energy transfer arising from dynamical interactions between the subgrid scales and the resolved scales $k < k' < k_m$: ——, $k_m\eta = 0.18$; · · · · · ·, $k_m\eta = 0.39$.

i.e. from local interactions near the cutoff. The observed dominance of local energy exchanges in the overall dynamics of transfer is consistent with classical models of the energy cascade (Tennekes & Lumley 1972) and results from recent investigations of detailed triadic interactions in turbulence (Domaradzki & Rogallo 1990; Ohkitani & Kida 1992; Waleffe 1992; Zhou 1993), which have all shown the predominance of local energy exchanges in the dynamics of turbulence.

4. Subgrid-scale interactions in the physical space

In the physical space, the transfer of energy between the subgrid scales and the resolved flow can be represented as (see Appendix B)

$$T_S(\boldsymbol{x},t) = -\frac{\partial}{\partial x_\beta}(u_\alpha^{\mathscr{L}}\tau_{\alpha\beta}) - \frac{\partial}{\partial x_\alpha}(u_\alpha^{\mathscr{L}}p^{\mathscr{L}|\mathscr{S}}) - \epsilon_S(\boldsymbol{x},t), \tag{4.1}$$

where

$$\epsilon_S(\boldsymbol{x},t) = -\tau_{\alpha\beta}S_{\alpha\beta}^{\mathscr{L}} \tag{4.2}$$

denotes the subgrid-scale dissipation, $\tau_{\alpha\beta}(\boldsymbol{x},t) = (u_\alpha u_\beta - u_\alpha^{\mathscr{L}}u_\beta^{\mathscr{L}})^{\mathscr{L}}$ is the (true) subgrid-scale stress, and $S_{\alpha\beta}^{\mathscr{L}} = \frac{1}{2}(\partial u_\alpha^{\mathscr{L}}/\partial x_\beta + \partial u_\beta^{\mathscr{L}}/\partial x_\alpha)$ is the large-scale deformation tensor. Studies of subgrid-scale energy transfer in physical space have traditionally ignored the effect of the redistribution terms in (4.1) and concentrated on the properties

FIGURE 5. The spectral eddy-viscosity, $\nu_w(k|k_m;k_t)$, acting on a scale k due to dynamical interactions with wavenumbers $k_m < k' \leqslant k_t$ for $k_m\eta = 0.18$ and (*a*) $k_t/k_m = 2.0$, (*b*) $k_t/k_m = 1.5$, and (*c*) $k_t/k_m = 1.25$. Also shown are $\nu_w(k|k_m)$ in the full field and the breakdown of $\nu_w(k|k_m;k_t)$ and $\nu_w(k|k_m)$ into forward and reverse contributions. —□—, $\nu_w(k|k_m;k_t)$; · ·⊡· ·, $\nu_w^+(k|k_m;k_t)$; — —□— —, $\nu_w^-(k|k_m;k_t)$; ——, $\nu_w(k|k_m)$; · · · · · ·, $\nu_w^+(k|k_m)$; — — —, $\nu_w^-(k|k_m)$.

https://doi.org/10.1017/S0022112099007582 Published online by Cambridge University Press

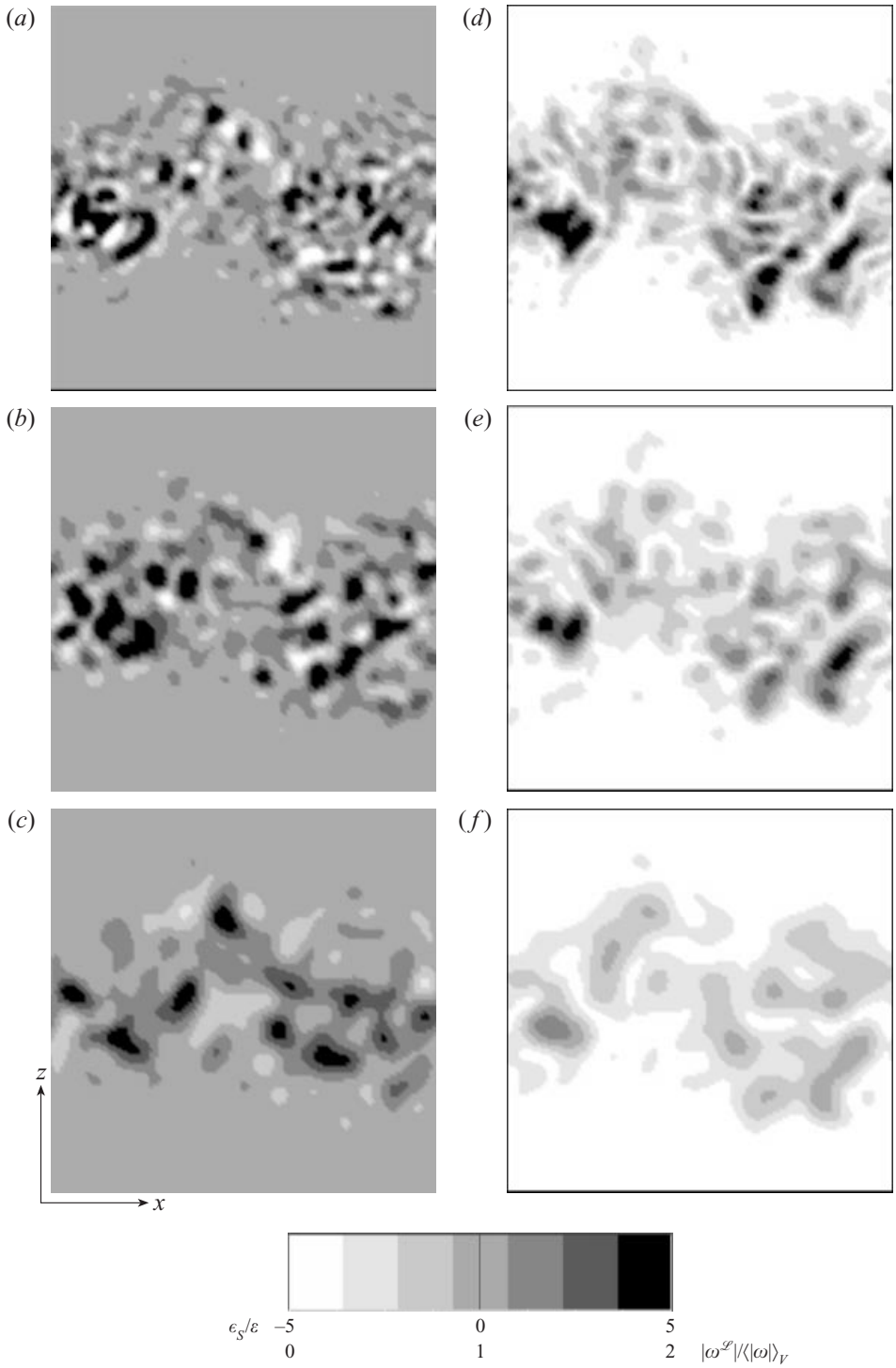


FIGURE 7. Spatial distributions of (*a–c*) subgrid-scale dissipation, ϵ_S, and (*d–f*) resolved-scale vorticity magnitude, $|\omega^{\mathscr{L}}|$, in a planar cut through the jet for three cutoff wavenumbers in the inertial range: (*a, d*) $k_m\eta = 0.18$; (*b, e*) $k_m\eta = 0.135$; (*c, f*) $k_m\eta = 0.08$.

https://doi.org/10.1017/S0022112099007582 Published online by Cambridge University Press

of the subgrid-scale dissipation. In keeping with this tradition, we will also base our discussion on the subgrid-scale dissipation, $\epsilon_S(\boldsymbol{x}, t)$, instead of the total transfer, $T_S(\boldsymbol{x}, t)$.

Figure 7 shows the spatial distributions of subgrid-scale dissipation, $\epsilon_S(\boldsymbol{x}, t)$, in a planar cut through the jet for three cutoff wavenumbers $k_m\eta = 0.18$, 0.135, and 0.08 (all in the inertial range). Also shown are the spatial distributions of the resolved-scale vorticity field in the same planes. The subgrid-scale dissipation field is composed of coherent regions of intense forward and reverse energy transfer, which are superimposed on a background of low-intensity forward transfer. The former are the physical-space embodiments of the cusps in the spectral eddy viscosity, the latter represent the low-wavenumber asymptote. The intense regions of forward and reverse transfer have a scale on the order of the width of the cutoff filter and are spatially correlated with the organized vortical structures at that scale, occurring at the periphery of these structures. This suggests the mutual straining of these vortical structures as a possible origin of these transfers. The coherent and scale-dependent nature of these transfers implies that they cannot be modelled as a stochastic force as has been suggested in a number of recent studies (Bertoglio 1985; Chasnov 1991; Leith 1990; Mason & Thomson 1992; Schumann 1995; Carati *et al.* 1995).

The dynamical origin of these intense transfers can be determined by examining the structure of the subgrid-scale dissipation field, $\epsilon^t_S(\boldsymbol{x}, t) = -\tau^t_{\alpha\beta} S^{\mathscr{L}}_{\alpha\beta}$, in truncated databases of the velocity field. Here, $\tau^t_{\alpha\beta}(\boldsymbol{x}, t) = (\check{u}_\alpha \check{u}_\beta - u^{\mathscr{L}}_\alpha u^{\mathscr{L}}_\beta)^{\mathscr{L}}$ represents the subgrid-scale stress in the truncated database and $\check{u}_\alpha(\boldsymbol{x}, t)$ is the truncated velocity field, obtained from the full field by setting all modes with a wavenumber greater than k_t equal to zero. Figure 8 shows $\epsilon^t_S(\boldsymbol{x}, t)$ with $k_m\eta = 0.18$ and $k_t/k_m = 2.0$, 1.5, and 1.25 in the same plane as that shown in figure 7(*a*). Also shown is the structure of the residual field, $\epsilon^r_S(\boldsymbol{x}, t) = \epsilon_S - \epsilon^t_S$ in the same planes. For all three values of k_t/k_m, the subgrid-scale dissipation in the truncated field is visually indistinguishable from that in the non-truncated field (shown in figure 7*a*). This indicates that these intense transfers are the result of interactions between the resolved scales and only the narrow band of subgrid wavenumbers between $k_m < k < 1.25k_m$. The additional modes $k > 1.25k_m$ mainly contribute to the background forward transfer.

These conclusions can be quantified by examining the profiles of the mean subgrid-scale dissipation fields $\langle \epsilon_S \rangle$ and $\langle \epsilon^t_S \rangle$ in the jet. Figure 9 shows $\langle \epsilon_S \rangle$ and $\langle \epsilon^t_S \rangle$, together with the breakdown of each into forward and reverse transfers, for $k_m\eta = 0.18$ and $k_t/k_m = 2.0$, 1.5, and 1.25. For all three k_t/k_m, elimination of the subgrid-scale modes $k > k_t$ reduces the background forward transfer from its full field value. For $k_t/k_m = 1.5$, the modes $k > k_t$ contribute 30% of the net subgrid-scale dissipation, while for $k_t/k_m = 1.25$ they contribute 40%. However, the mean distribution of backscatter is virtually unchanged from that in the full field. This, once again, verifies that backscatter is the result of local interactions between the resolved scales and only a very narrow band of subgrid wavenumbers between $k_m < k < 1.25k_m$.

5. Implications for subgrid-scale modelling

The results discussed in §3 and §4 imply that in modelling the subgrid-scale interactions two separate effects should be included: one representing the non-local interactions, which give rise to the low-wavenumber asymptote of the spectral eddy viscosity and the low-intensity forward transfers of energy in physical space; the other representing the local interactions near the cutoff, which give rise to the cusps in the spectral eddy viscosity and the intense and coherent regions of forward and

https://doi.org/10.1017/S0022112099007582 Published online by Cambridge University Press

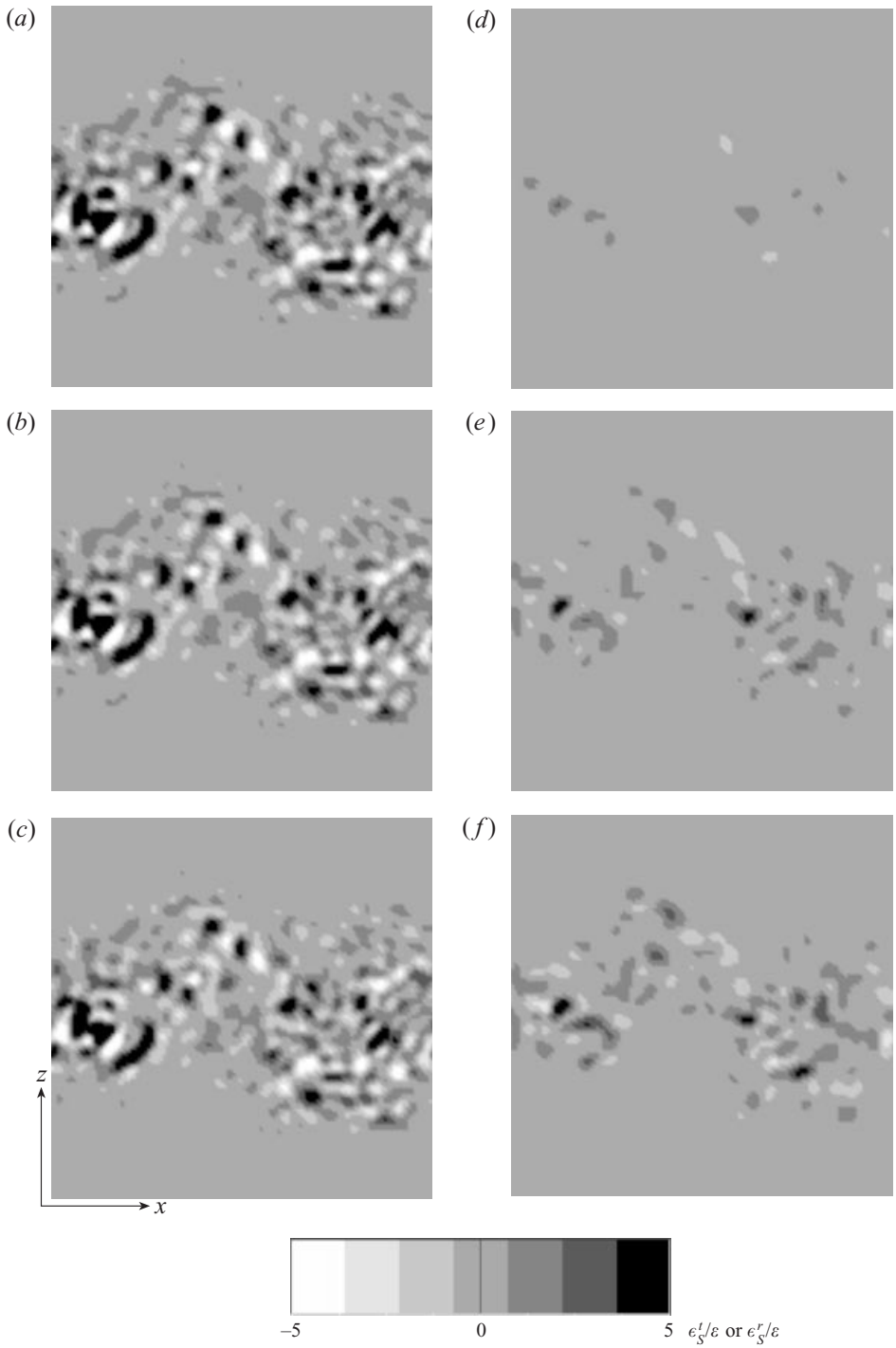


FIGURE 8. Spatial distributions of (*a–c*) the truncated subgrid-scale dissipation, ϵ_S^t, and (*d–f*) the residual fields, $\epsilon_S^r = \epsilon_S - \epsilon_S^t$, in the jet for $k_m\eta = 0.18$ and (*a*, *d*) $k_t/k_m = 2.0$; (*b*, *e*) $k_t/k_m = 1.5$; (*c*, *f*) $k_t/k_m = 1.25$.

https://doi.org/10.1017/S0022112099007582 Published online by Cambridge University Press

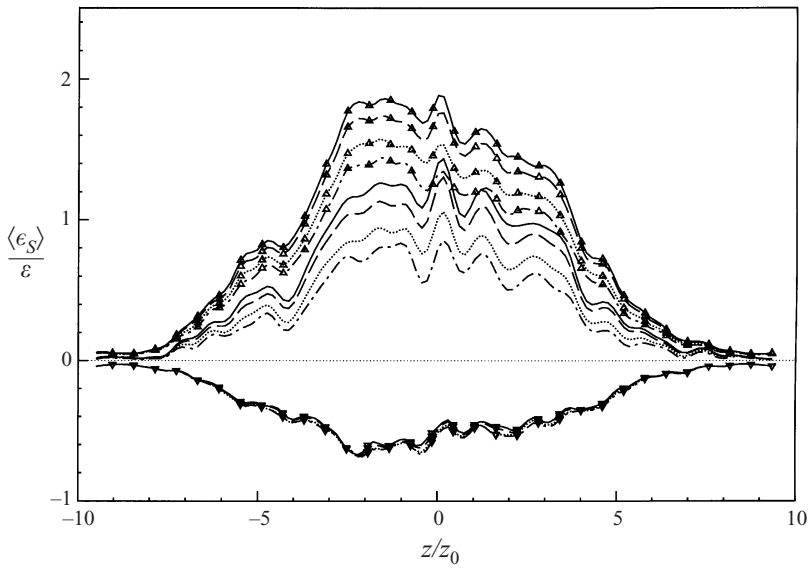


FIGURE 9. Profiles of the mean subgrid-scale dissipation, $\langle \epsilon_S \rangle$ and $\langle \epsilon_S^t \rangle$, in the full and truncated databases of the velocity field in the jet for $k_m\eta = 0.18$ and $k_t/k_m = 2.0$, 1.5, and 1.25. Also shown are the breakdown of $\langle \epsilon_S \rangle$ and $\langle \epsilon_S^t \rangle$ into forward (denoted by $\triangle$) and reverse (denoted by $\triangledown$) transfers of energy. ——, Full field; — — —, $k_t/k_m = 2.0$; · · · · · ·, $k_t/k_m = 1.5$; — · —, $k_t/k_m = 1.25$.

reverse transfer in the physical space. The former can be modelled by an eddy-viscosity parameterization, the latter can be represented by the interactions between the resolved scales and a narrow band of subgrid wavenumbers between $k_m < k < k_t$, where $k_t/k_m \sim 1.25$. This suggests a 'two-component' parameterization of the (true) subgrid-scale stress of the form

$$\tau^*_{\alpha\beta} = -2\nu_t S^{\mathscr{L}}_{\alpha\beta} + \tau'^*_{\alpha\beta}, \tag{5.1}$$

where $*$ denotes the deviatoric part of the stress tensor, ν_t is an eddy viscosity, $S^{\mathscr{L}}_{\alpha\beta} = \frac{1}{2}(\partial u^{\mathscr{L}}_\alpha/\partial x_\beta + \partial u^{\mathscr{L}}_\beta/\partial x_\alpha)$ is the large-scale strain rate, and $\tau'_{\alpha\beta}$ represents the (true) subgrid-scale stress arising from interactions with the subgrid modes $k_m < k < k_t$. In this section, we describe the development of this model for sharp (Fourier) filters. The extension to graded filters is discussed in § 8.

For sharp (Fourier) filters, the true SGS stress is given by $\tau_{\alpha\beta} = (u_\alpha u_\beta - u^{\mathscr{L}}_\alpha u^{\mathscr{L}}_\beta)^{\mathscr{L}}$ and $\tau'_{\alpha\beta}$ given by the SGS stress arising from the truncated velocity field

$$\tau'_{\alpha\beta} = \tau^t_{\alpha\beta} = (\check{u}_\alpha \check{u}_\beta - u^{\mathscr{L}}_\alpha u^{\mathscr{L}}_\beta)^{\mathscr{L}}, \tag{5.2}$$

where $\check{u}_\alpha(\boldsymbol{x}, t)$ represents the velocity field truncated to (filtered at) k_t.

The parameterization of ν_t can be obtained from the low-wavenumber asymptote of the spectral eddy viscosity. Since this asymptote has a constant magnitude, its physical-space representation is also given by

$$\nu_t = \nu(0|k_m). \tag{5.3}$$

The results shown in figure 4 as well as those provided by analytical theories of turbulence (Kraichnan 1976; Chollet & Lesieur 1981) show this low-wavenumber

https://doi.org/10.1017/S0022112099007582 Published online by Cambridge University Press

asymptote to have a magnitude

$$v(0|k_m) = 0.44 C_K^{-3/2} \sqrt{\frac{E(k_m)}{k_m}}, \tag{5.4}$$

where $E(k_m)$ is the turbulence kinetic energy at scale k_m and C_K is the Kolmogorov constant. This expression becomes equivalent to the classical Smagorinsky (1963) model if $E(k_m)$ is expressed in terms of the large-scale strain-rate tensor. While this is the representation adopted in this study, this approach is not unique and other eddy-viscosity models (e.g. Kwak *et al.* 1975; Metais & Lesieur 1992) can be derived in a similar fashion by expressing $E(k_m)$ in terms of other large-scale properties of the flow. To recover the Smagorinsky model, we assume an LES cutoff k_m in the inertial range such that $E(k_m) = C_K \varepsilon^{2/3} k_m^{-5/3}$ and note that the average rate of kinetic energy dissipation can be expressed as $\varepsilon = C' v(0|k_m) \langle 2 S^{\mathscr{L}}_{\alpha\beta} S^{\mathscr{L}}_{\alpha\beta} \rangle_V$. Thus, equation (5.4) can be written as

$$v_t = v(0|k_m) = C'' \overline{\Delta}^2 \langle 2 S^{\mathscr{L}}_{\alpha\beta} S^{\mathscr{L}}_{\alpha\beta} \rangle_V^{1/2}, \tag{5.5}$$

where $C'' = C'^{1/2} 0.44^{3/2} / (\pi^2 C_K^{3/2})$, $\overline{\Delta} = \pi / k_m$, and $\langle \cdot \rangle_V$ denotes a volume average. This reduces to the classical Smagorinsky (1963) model, if it is further assumed that at the scale k_m of the LES filter the volume average of $\langle 2 S^{\mathscr{L}}_{\alpha\beta} S^{\mathscr{L}}_{\alpha\beta} \rangle_V^{1/2}$ is not too different from its local value $|S^{\mathscr{L}}| = (2 S^{\mathscr{L}}_{\alpha\beta} S^{\mathscr{L}}_{\alpha\beta})^{1/2}$. With this approximation, the 'two-component' parameterization (5.1) and (5.2) can be written as

$$\tau^*_{\alpha\beta} = -2C \overline{\Delta}^2 |S^{\mathscr{L}}| S^{\mathscr{L}}_{\alpha\beta} + (\check{u}_\alpha \check{u}_\beta - u^{\mathscr{L}}_\alpha u^{\mathscr{L}}_\beta)^{\mathscr{L}*}, \tag{5.6}$$

or in the more customary notation of LES, where the large-scale quantities are denoted by an overbar,

$$\tau^*_{ij} = -2C \overline{\Delta}^2 |\overline{S}| \overline{S}_{ij} + (\overline{\check{u}_i \check{u}_j} - \overline{\overline{u}_i \overline{u}_j})^*, \tag{5.7}$$

where $\tau_{ij} = \overline{u_i u_j} - \overline{\overline{u}_i \overline{u}_j}$ is the true subgrid-scale stress and the overbar denotes a sharp (Fourier) filter at k_m.

Implicit in this parameterization is the assumption that the spatial variability in the subgrid-scale transfer is captured in the local-interactions term τ'_{ij}, so that v_t or C are nearly constant in space. To test the validity of this hypothesis, we compare the p.d.f. of the model coefficient, C, obtained in the jet with the 'two-component' parameterization (5.7) to the p.d.f. of C based on a pure Smagorinsky parameterization. Figure 10 shows these results for a cutoff filter at $k_m \eta = 0.18$ and three values of $k_t / k_m = 2.0$, 1.5 and 1.25. The model coefficients were computed using a least-squares method according to

$$C = -\frac{(\tau_{ij} - \tau'_{ij}) \overline{S}_{ij}}{2 \overline{\Delta}^2 |\overline{S}| \overline{S}_{ij} \overline{S}_{ij}},$$

where τ'_{ij} is set equal to zero in the pure Smagorinsky parameterization. For all three values of k_t / k_m, the inclusion of the local-interactions term results in a considerably narrower distribution of model coefficient values than a pure Smagorinsky model, verifying that the model is consistent with its underlying assumptions.

In applying the 'two-component' parameterization (5.7) to LES, one is faced with two problems: (i) the subgrid modes $k_m < k < k_t$ required for the computation of $\check{u}_i$ are not available in a LES with a sharp (Fourier) filter where the LES filter is at k_m, and (ii) the coefficient C is not known. The first issue can be resolved by exploiting two properties of the local interactions, namely that they involve only a very narrow

https://doi.org/10.1017/S0022112099007582 Published online by Cambridge University Press

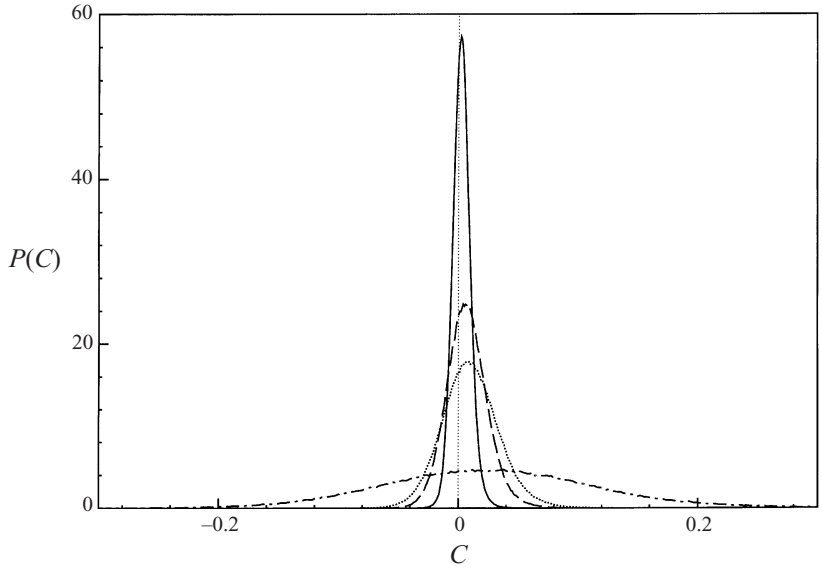


FIGURE 10. Probability density function of the model coefficient C from parameterization (5.7) compared to a pure Smagorinsky parameterization for $k_m\eta = 0.18$ and ——, $k_t/k_m = 2.0$; – – –, $k_t/k_m = 1.5$; · · · · ·, $k_t/k_m = 1.25$; – · –, Smagorinsky model.

band of subgrid wavenumbers, and arise from mutual straining of coherent eddies so that they have similar structures at neighbouring cutoffs. The latter feature is demonstrated in the structure of the subgrid-scale dissipation fields at neighbouring cutoffs $k_m\eta = 0.18$, 0.135 and 0.09 shown in figure 7 (the full-domain correlation coefficients between the dissipation fields at successive cutoffs is ~ 0.35). Together, these two features suggest that the local interactions at cutoff k_m can be approximated by those at a neighbouring cutoff $\widetilde{k} = k_m/b$ where $b > 1$. In other words, the local interactions between the resolved scales $k < k_m$ and subgrid modes $k_m < k < k_t$ can be approximated by those between the resolved scales $k < \widetilde{k}$ and $\widetilde{k} < k < k_m$. The value of b should be large enough so the local interactions are properly represented, but small enough so the two fields at $\widetilde{k}$ and k_m remain correlated. Based on the results presented in figures 5–9, these requirements are satisfied with $b \sim 1.25$. In our computations we use a value of $b = \frac{4}{3}$. However, the results are not too sensitive to the precise value of b.

With these approximations, equation (5.7) can be replaced with

$$\tau^*_{ij} = -2C\overline{\Delta}^2|\overline{S}|\overline{S}_{ij} + (\widetilde{\overline{u}_i\overline{u}_j} - \widetilde{\overline{u}_i}\widetilde{\overline{u}_j})^*, \tag{5.8}$$

where the tilde denotes a sharp (Fourier) filter at $\widetilde{k}$. The model coefficient C in (5.8) is determined using the dynamic procedures suggested by Germano *et al.* (1991) and Lilly (1992). To implement this, a test filter is applied at the resolved scale $\widehat{k} = k_m/a$, where a is taken to be 2.0 as recommended by Germano *et al.* (1991), and the subgrid-scale stress $T_{ij} = \widehat{u_iu_j} - \widehat{u}_i\widehat{u}_j$ at this scale is parameterized using the 'two-component' model (5.7)

$$T^*_{ij} = -2C\widehat{\Delta}^2|\widehat{S}|\widehat{S}_{ij} + (\widehat{\overline{u}_i\overline{u}_j} - \widehat{\overline{u}_i}\widehat{\overline{u}_j})^*, \tag{5.9}$$

where $\widehat{\Delta} = \pi/\widehat{k}$. Note that in parameterizing T_{ij}, the modes $\widehat{k} < k < k_m$ required

https://doi.org/10.1017/S0022112099007582 Published online by Cambridge University Press

for the construction of the local-interactions term, T'_{ij}, are available and there is no need to approximate this term as was done for τ_{ij}. The coefficient $C(\boldsymbol{x},t)$ is then determined using the least-squares method suggested by Lilly (1992). This gives the model coefficient as

$$C(\boldsymbol{x},t) = -\frac{\mathscr{D}_{ij}M_{ij}}{2M_{ij}M_{ij}}, \tag{5.10}$$

where

$$\mathscr{D}_{ij} = \widehat{\overline{u}_i\overline{u}_j} - \widehat{\widetilde{u}_i\widetilde{u}_j}, \tag{5.11}$$

and

$$M_{ij} = \widehat{\Delta}^2|\widehat{\overline{S}}|\widehat{\overline{S}}_{ij} - \overline{\Delta}^2\widehat{|\overline{S}|\overline{S}_{ij}}, \tag{5.12}$$

and it has been assumed that the variation of $C(\boldsymbol{x},t)$ at the level of the test filter is small so it can be taken out of the filtering operation.

The dynamic two-component model (DTM) given by equations (5.8) and (5.10)–(5.12) for sharp (Fourier) filters offers a number of advantages over pure eddy-viscosity parameterizations. In particular, the model is applicable at a local level and naturally accounts for backscatter based on the dynamics of the resolved scales. Unlike dynamic eddy-viscosity models, DTM does not require any averaging in space or time in the expression for the model coefficient. This is because the eddy-viscosity term is used only to account for the low-intensity forward transfers of energy, while the intense forward and reverse transfers are represented by the local-interactions term. This significantly reduces the variability in the model coefficient. The inclusion of the local-interactions term also provides a natural means of accounting for backscatter.

6. Model evaluation by *a priori* tests

The performance of the dynamic two-component model given by equations (5.8) and (5.10)–(5.12) was evaluated in *a priori* tests using the DNS database of the jet at time $tU_0/z_0 = 100$. The results are compared to DNS, the classical Smagorinsky model (SM) given by

$$\tau^*_{ij} = -2C\overline{\Delta}^2|\overline{S}|\overline{S}_{ij}, \tag{6.1}$$

where $C = 0.01$, and the dynamic Smagorinsky model (DSM) (Germano *et al.* 1991; Lilly 1992) given by (6.1), where

$$C = -\frac{\langle\mathscr{F}_{ij}M_{ij}\rangle}{2\langle M_{ij}M_{ij}\rangle}, \tag{6.2}$$

$$\mathscr{F}_{ij} = \widehat{\overline{u}_i\overline{u}_j} - \widehat{\widehat{u}_i\widehat{u}_j}, \tag{6.3}$$

$$M_{ij} = \widehat{\Delta}^2|\widehat{\overline{S}}|\widehat{\overline{S}}_{ij} - \overline{\Delta}^2\widehat{|\overline{S}|\overline{S}_{ij}}, \tag{6.4}$$

and $\langle\cdot\rangle$ denotes averaging in the homogeneous (x,y) directions. This averaging is needed in DSM to avoid large negative values of C, which are unphysical and can lead to numerical instability in practice (Germano *et al.* 1991; Lund *et al.* 1993). The *a priori* tests were performed using sharp (Fourier) filters applied with the same filter widths in all three directions. To facilitate filtering in the lateral direction, the jet was truncated to $-3.2 < z/z_m < 3.2$ and the data interpolated onto a uniform Fourier grid. The LES filter $\overline{G}$ was applied at $k_m\eta = 0.18$, and the auxiliary filters $\widehat{G}$ and $\widetilde{G}$

https://doi.org/10.1017/S0022112099007582 Published online by Cambridge University Press

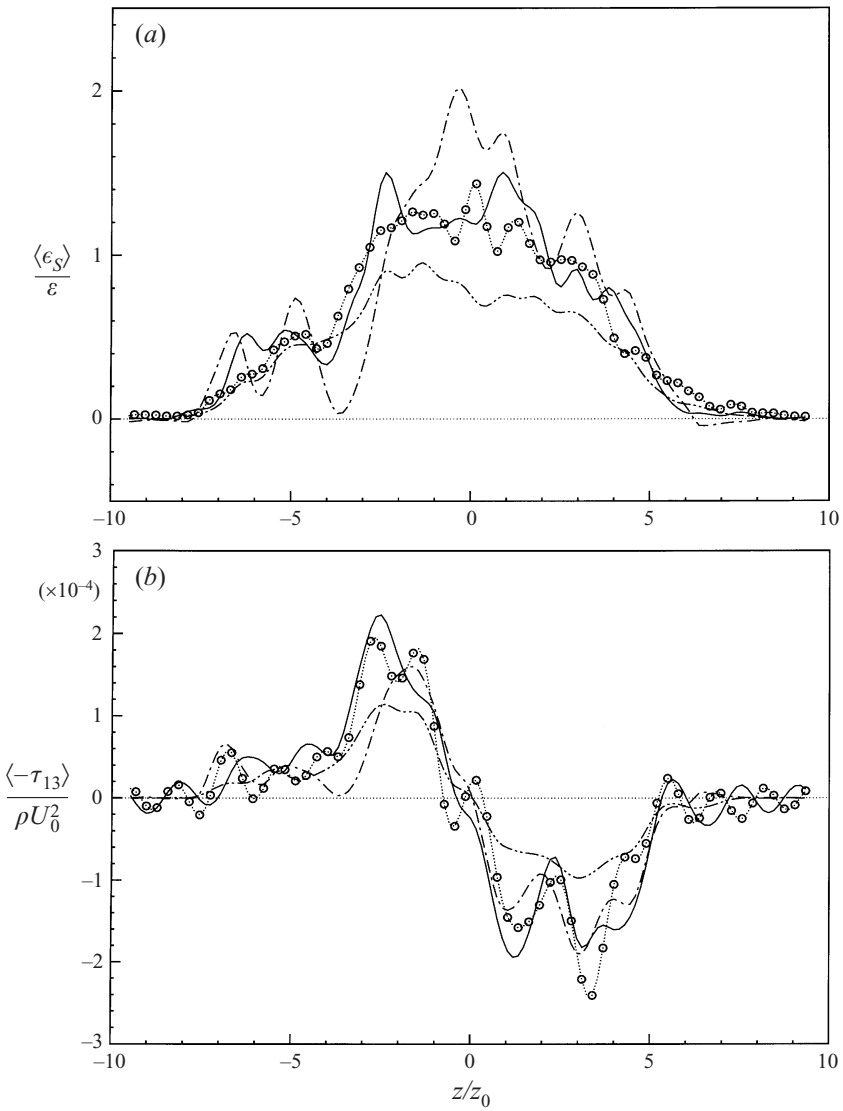


FIGURE 11. Profiles of (*a*) mean subgrid-scale dissipation, and (*b*) mean subgrid-scale stress fields predicted in *a priori* tests compared to DNS: · · O · ·, DNS; ——, DTM; — · —, DSM; — · ·—, Smagorinsky model (with $C = 0.01$).

were applied at $\widehat{k}/k_m = 0.5$ and $\widetilde{k}/k_m = 0.75$, respectively. The filter widths $\overline{\Delta}$ and $\widehat{\Delta}$ were defined as the geometric mean of the uni-directional filters.

Figure 11 shows the predictions of these models for the mean subgrid-scale dissipation, $\langle \epsilon_S \rangle$, and the mean subgrid-scale stress, $\langle -\tau_{13} \rangle$, in the jet, compared to DNS results. Both DTM and DSM give reasonably accurate predictions of these mean quantities, with DTM giving slightly better results.

In addition to the mean quantities, DTM also correctly predicts the breakdown of the net transfer into forward and reverse contributions. This is a major shortcoming of pure eddy-viscosity models, which are inherently 'averaged' and as such can only yield the net transfer. The predictions of DTM for the net subgrid-scale dissipation,

https://doi.org/10.1017/S0022112099007582 Published online by Cambridge University Press

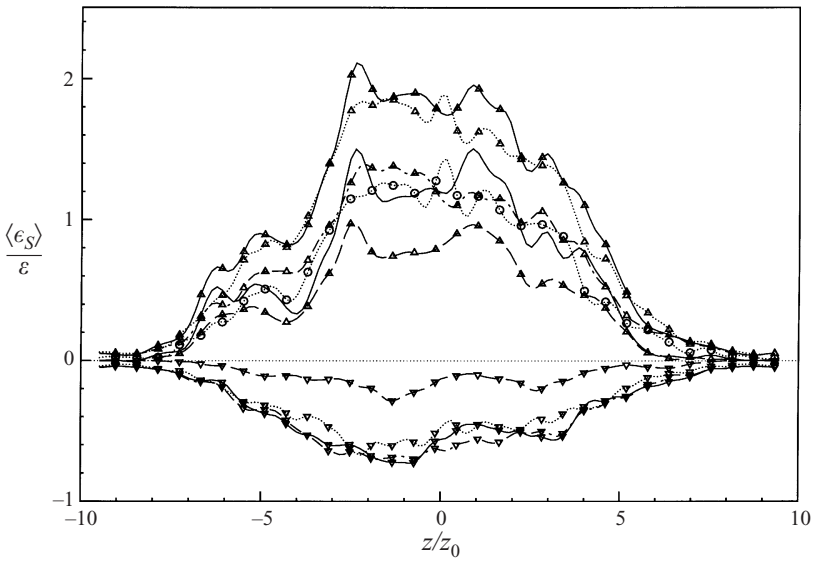


FIGURE 12. The net subgrid-scale dissipation and its breakdown into forward (denoted by △) and reverse (denoted by ▽) transfers predicted by DTM in *a priori* tests compared to DNS. Also shown are the contributions of each of the 'local-interactions' and 'eddy-viscosity' terms in DTM to forward (△) and reverse (▽) transfers. · · ○ · ·, DNS; ——, DTM; — — —, eddy-viscosity term in DTM; — · —, local-interactions term in DTM.

$\langle \epsilon_S \rangle$, and its breakdown into forward, $\langle \epsilon_S^+ \rangle$, and reverse, $\langle \epsilon_S^- \rangle$, contributions are compared to DNS results in figure 12. Also shown are the contributions of each of the local-interactions and eddy-viscosity terms in DTM to these forward and reverse transfers. The model predictions agree with the DNS results for both the net subgrid-scale dissipation and its breakdown into forward and reverse transfers. The eddy-viscosity and local-interactions terms each contribute nearly equally (48% and 52%, respectively) to the forward transfers, while the reverse transfers are almost entirely accounted for by the local-interactions term. There is also a small reverse transfer arising from the eddy-viscosity term, reflecting the presence of negative values of C in the domain. In LES applications, this contribution is removed based on the argument that the role of the eddy-viscosity term in DTM is to account for forward transfers of energy, not backscatter. Accordingly, at each time-step we set $\nu_t = 0$ wherever it becomes negative, and account for the energy associated with these reverse transfers by uniformly weighting the eddy viscosity in regions of positive ν_t such that the net SGS dissipation in the domain by the eddy viscosity remains the same. The latter step is only a small correction, as the energy associated with negative values of ν_t is small. Nevertheless, it results in a marginal improvement (on the order of $\sim 5\%$) in the predicted LES statistics.

Figure 13 shows the p.d.f. of the model coefficient in DTM (equation (5.10)) compared to that which would be obtained in DSM without averaging (equation (6.2) without any averaging of the numerator or the denominator). The inclusion of the local-interactions term in DTM significantly reduces the variability of the model coefficient compared to DSM. This eliminates the need for averaging the model coefficient. The negative values of C occurring in DTM for the most part (in $\sim 90\%$ of the points) have a small magnitude such that $\nu + C\overline{\Delta}^2|\overline{S}|$ remains positive. Nevertheless, in view of the role of the eddy-viscosity term in DTM, all negative values

https://doi.org/10.1017/S0022112099007582 Published online by Cambridge University Press

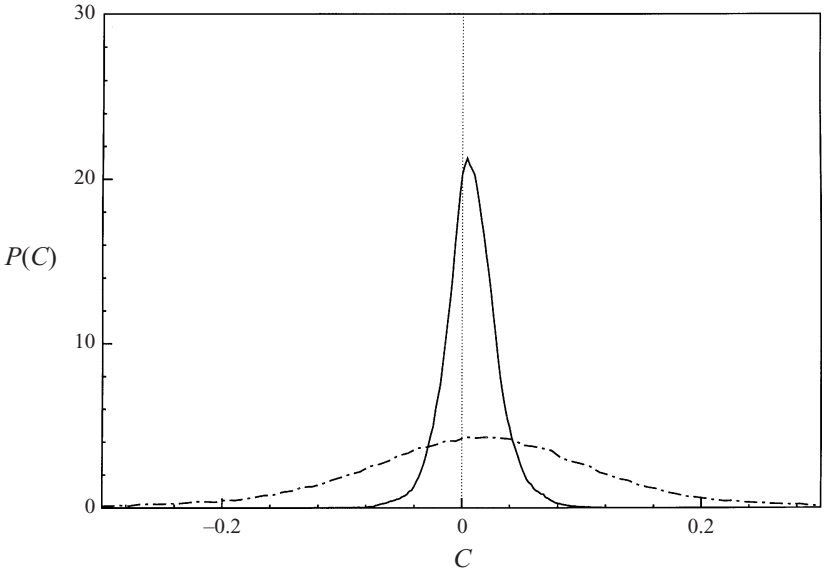


FIGURE 13. Probability density function of the model coefficient C in DTM compared to DSM (without any spatial averaging) predicted in *a priori* tests: ——, DTM; — · —, DSM.

of C are removed using the procedure described above. A more rigorous procedure for preventing negative values of C, such as one based on a constrained variational formulation (Ghosal *et al.* 1995), could be implemented. However, considering the additional complexity of this procedure and the insensitivity of the LES results to the details of this clipping, this has not been attempted here.

The local structure of the subgrid-scale dissipation field, $\epsilon_S = -\tau_{ij}\overline{S}_{ij}$, predicted by DTM is compared to results from DNS, DSM, and the Smagorinsky model in figure 14. The DTM predictions are in reasonable agreement with DNS and show regions of both forward and reverse transfer (the full-domain correlation coefficients between the two fields is ~ 0.3). In contrast, the subgrid-scale dissipation field predicted by DSM is essentially the same as that predicted by the classical Smagorinsky model and consists entirely of forward transfers of energy. The more accurate modelling of the local structure of the subgrid-scale dissipation field in DTM leads to improved predictions of the structures, spectra, and statistics in LES, and enhances the robustness of the model at marginal LES resolutions.

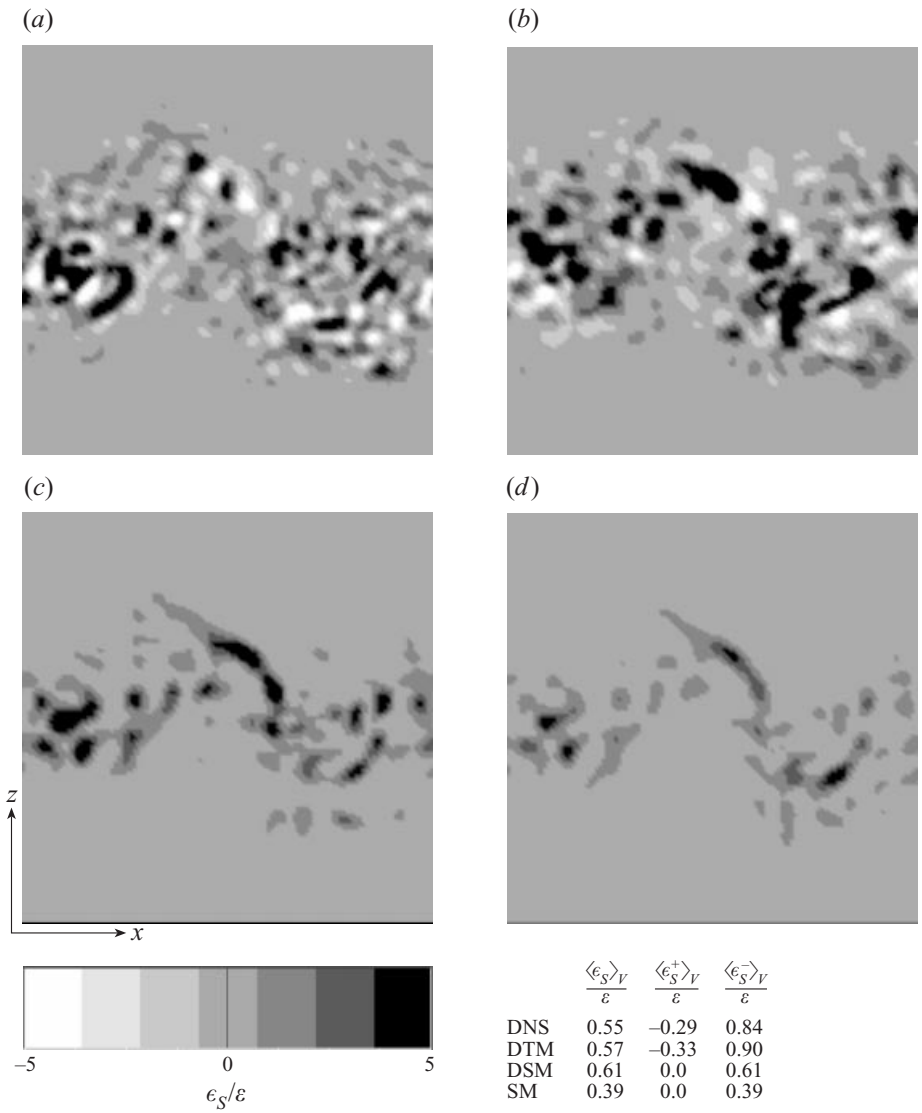
7. LES applications

7.1. *LES of transitional and turbulent flow in a jet*

As a first LES test case, we apply DTM to simulate the transitional and turbulent temporally growing planar jet flow described in § 2.1. The results are compared to those from DNS and LES with DSM. A coarse DNS (LES with no model) at the effective resolution of the LES is also performed to evaluate the effectiveness of the SGS models.

The simulations were performed using pseudo-spectral methods, and employed Fourier series in the homogeneous (x and y) directions and mapped Chebyshev polynomials in the lateral (z) direction. We solve the set of equations (1.2) and (1.5), with τ_{ij} given by (5.8) and (5.10)–(5.12) for DTM and (6.1)–(6.4) for DSM, and all

https://doi.org/10.1017/S0022112099007582 Published online by Cambridge University Press



	$\frac{\langle \epsilon_S \rangle_V}{\varepsilon}$	$\frac{\langle \epsilon_S^+ \rangle_V}{\varepsilon}$	$\frac{\langle \epsilon_S^- \rangle_V}{\varepsilon}$
DNS	0.55	–0.29	0.84
DTM	0.57	–0.33	0.90
DSM	0.61	0.0	0.61
SM	0.39	0.0	0.39

FIGURE 14. Local structure of the subgrid-scale dissipation field in a planar cut through the jet predicted by *a priori* tests for $k_m\eta = 0.18$ compared to DNS: (*a*) DNS, (*b*) DTM, (*c*) DSM, and (*d*) Smagorinsky model (with $C = 0.01$). Also tabulated are the volume averages $\langle \epsilon_S \rangle_V$, $\langle \epsilon_S^+ \rangle_V$ and $\langle \epsilon_S^- \rangle_V$ predicted by each model compared to DNS.

nonlinear terms represented in rotational form. The computations were performed with a resolution of $32 \times 32 \times 65$ and were de-aliased using the 1/2 rule, resulting in an effective resolution of $16 \times 16 \times 65$. The equations were advanced in time using the three-step splitting method suggested by Yakhot *et al.* (1989). The domain sizes in all three directions were the same as in DNS. Filtering was applied only in the homogeneous directions. The LES filter was applied at $\overline{k}_x = \overline{k}_y = 8$ and the auxiliary filters at $\widetilde{k}_i/\overline{k}_i = 0.75$ and $\widehat{k}_i/\overline{k}_i = 0.5$, respectively. The equivalent filter widths $\overline{\Delta}$ and $\widehat{\Delta}$ were defined as the geometric mean of the uni-directional filter widths. With these conditions, the LES filters had characteristic widths of $\overline{\Delta}_x = \overline{\Delta}_y = 32\eta$ and $\overline{\Delta}_z = 8\eta$.

https://doi.org/10.1017/S0022112099007582 Published online by Cambridge University Press

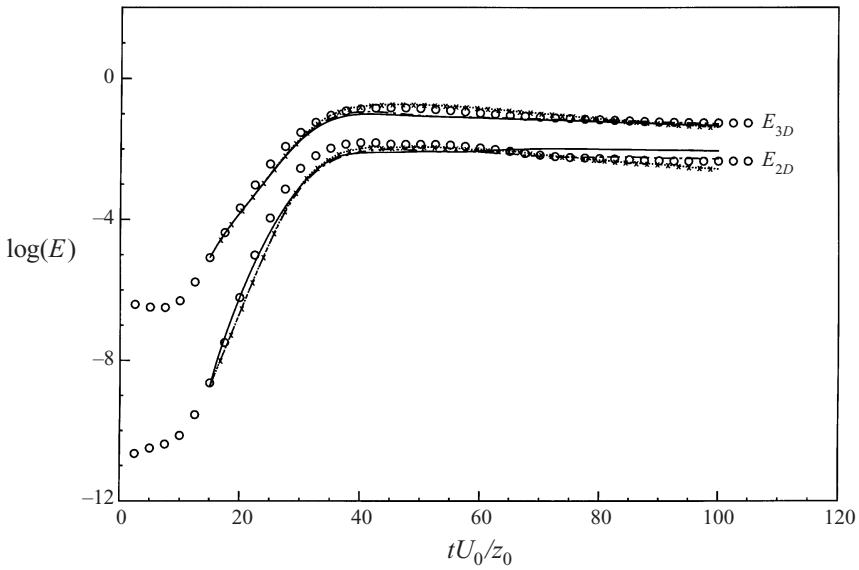


FIGURE 15. Time evolution of the kinetic energy of two- and three-dimensional disturbances in the jet predicted by LES compared to DNS: ○, DNS; ——, DTM; — · —, DSM; · · × · ·, no model.

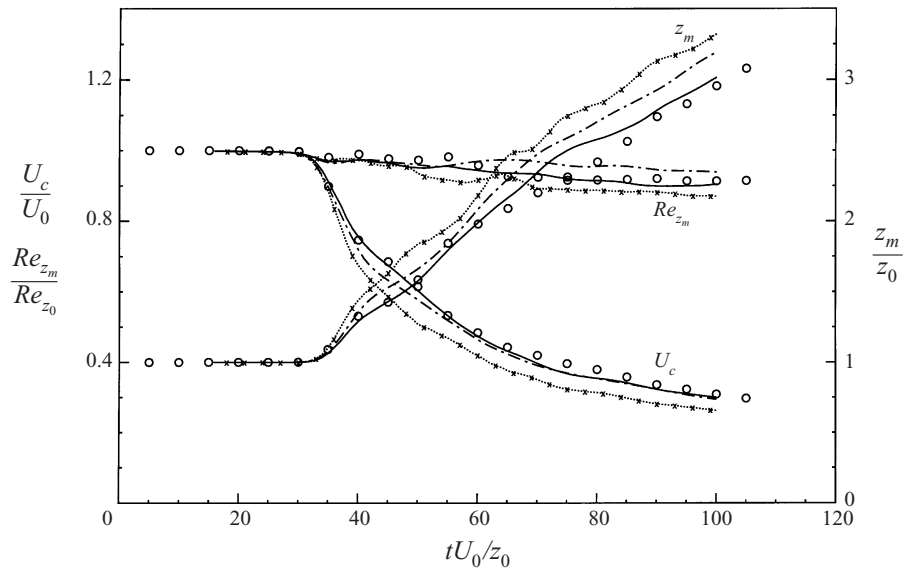


FIGURE 16. Time evolution of the jet half-width, jet centreline velocity, and jet Reynolds number predicted by LES compared to DNS: ○, DNS; ——, DTM; — · —, DSM; · · × · ·, no model.

Initial conditions for the LES runs were obtained from the DNS velocity field at the time $tU_0/z_0 = 15$.

The predictions of LES for the evolution of the energy of two- and three-dimensional disturbance fields, the jet half-width, $z_m(t)$, the jet centreline velocity, $U_c(t)$, and the jet Reynolds number, $Re_{z_m} = U_c z_m/\nu$, are compared to results from DNS in figures 15 and 16. The different stages in the evolution of the jet from its initially laminar state ($tU_0/z_0 < 30$) through the transition period ($30 < tU_0/z_0 < 60$)

https://doi.org/10.1017/S0022112099007582 Published online by Cambridge University Press

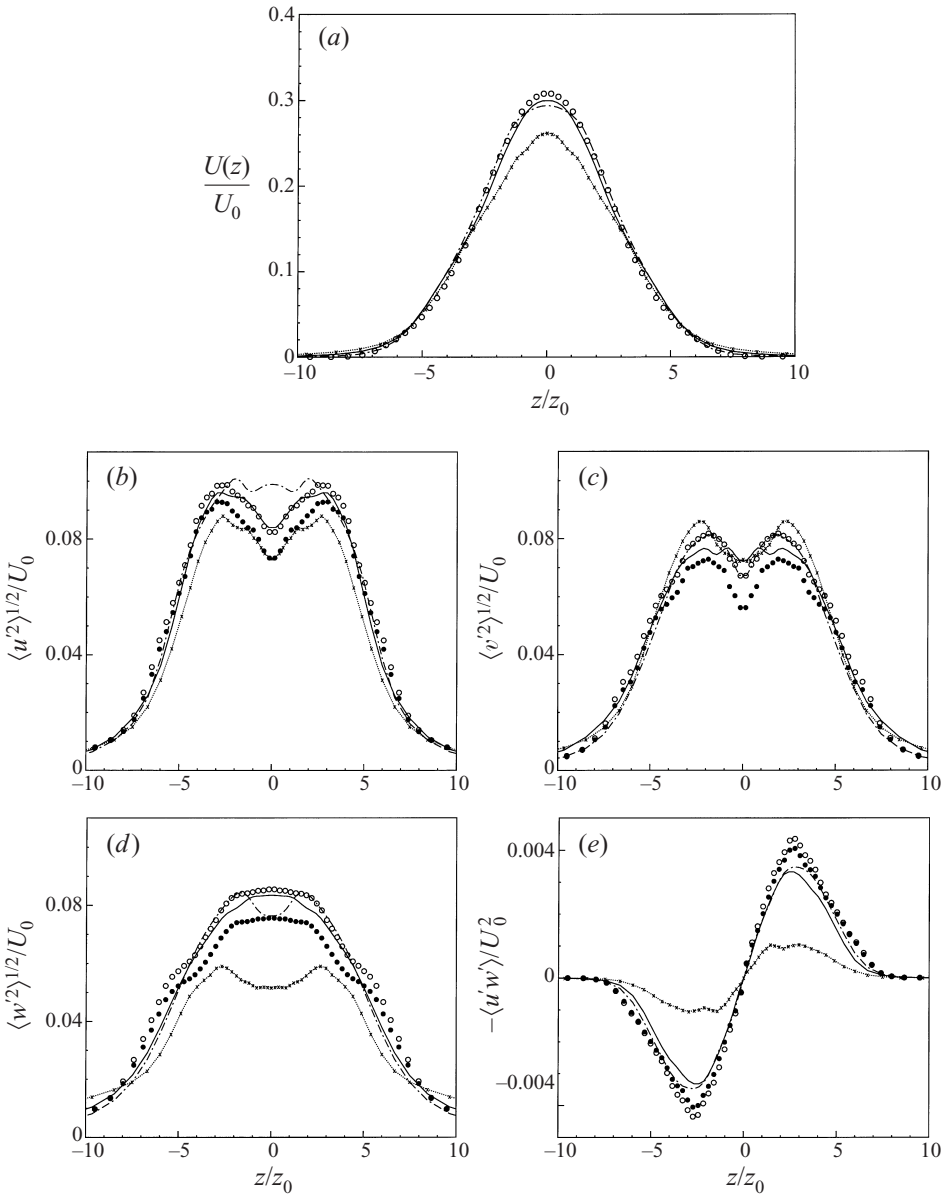


FIGURE 17. Mean turbulence statistics in the fully developed turbulent jet predicted by LES compared to DNS: ○, DNS; ●, filtered DNS; ——, DTM; — · —, DSM; · · × · ·, no model.

to the final equilibration into a fully developed turbulent state ($tU_0/z_0 > 70$) are displayed in these time histories. The overall energetics of the velocity fluctuations (figure 15) are fairly accurately predicted by both DTM and DSM. However, DTM provides the most accurate prediction of the mean structure of the jet (figure 16). DSM, as in no model, over-predicts the jet half-width and under-predicts its centreline velocity. Since the jet half-width and centreline velocity are controlled by the dynamics of the large-scale vortical structures in the flow, the success of DTM in predicting these quantities reflects its ability to correctly capture the large-scale vortical structure

https://doi.org/10.1017/S0022112099007582 Published online by Cambridge University Press

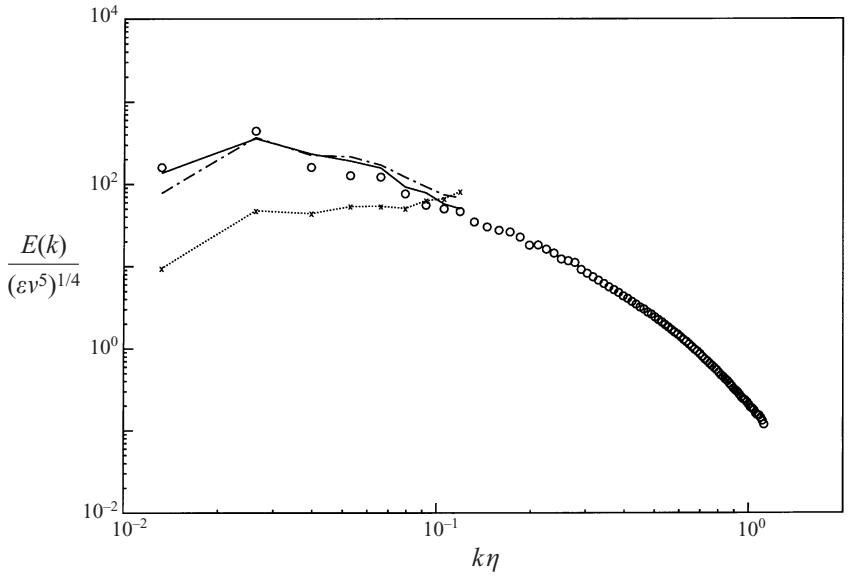


FIGURE 18. Three-dimensional kinetic energy spectrum in the fully developed turbulent jet predicted by LES compared to DNS: ○, DNS; ——, DTM; — · —, DSM; · · × · ·, no model.

of the jet. This is a consequence of the more accurate modelling of the local structure of the SGS dissipation field in DTM.

The mean turbulence statistics in the fully developed turbulent jet (at $tU_0/z_0 = 100$) are shown in figure 17. The results are compared to the DNS data filtered at the same conditions as those used in the LES. For reference, the unfiltered DNS data are also shown. DSM under-predicts the mean centreline velocity, over-predicts the turbulence intensities, and gives an incorrect shape for the distributions of the streamwise and lateral turbulence intensities in the central portion of the jet. All of these results are improved with DTM, which gives better agreement with the DNS results for both the mean velocity and the turbulence intensities and predicts the correct shape for the distributions of the turbulence intensities in the jet.

Figure 18 shows the three-dimensional kinetic energy spectrum in the fully developed turbulent jet (at $tU_0/z_0 = 100$). The best agreement with the DNS results is, once again, obtained with DTM. DSM under-predicts the disturbance kinetic energy at the low wavenumbers and over-predicts it at the high wavenumbers. This is expected and a consequence of the averaged nature of eddy-viscosity models. These models, in effect, approximate the true curve of the spectral eddy viscosity $\nu(k|k_m)$ (figure 4) by a k-independent average eddy viscosity, giving the same net dissipation. Such an averaged eddy viscosity is by construction over-dissipative at the low wavenumbers and under-dissipative at the high wavenumbers. DTM circumvents this problem by modelling the cusp separately from the low-wavenumber asymptote. This gives the model the ability to more accurately predict the modal distribution of the turbulence kinetic energy.

The difficulty experienced by DSM in capturing the dynamics of the jet can be attributed to its averaged nature. This seemingly simple flow in reality provides a stringent test of SGS models because its mean statistics are controlled by the dynamics of the large-scale vortical structures in the jet. Accurate prediction of these structures requires SGS models which are accurate at the local level. This is one area in which DTM provides an advantage over pure eddy-viscosity models.

https://doi.org/10.1017/S0022112099007582 Published online by Cambridge University Press

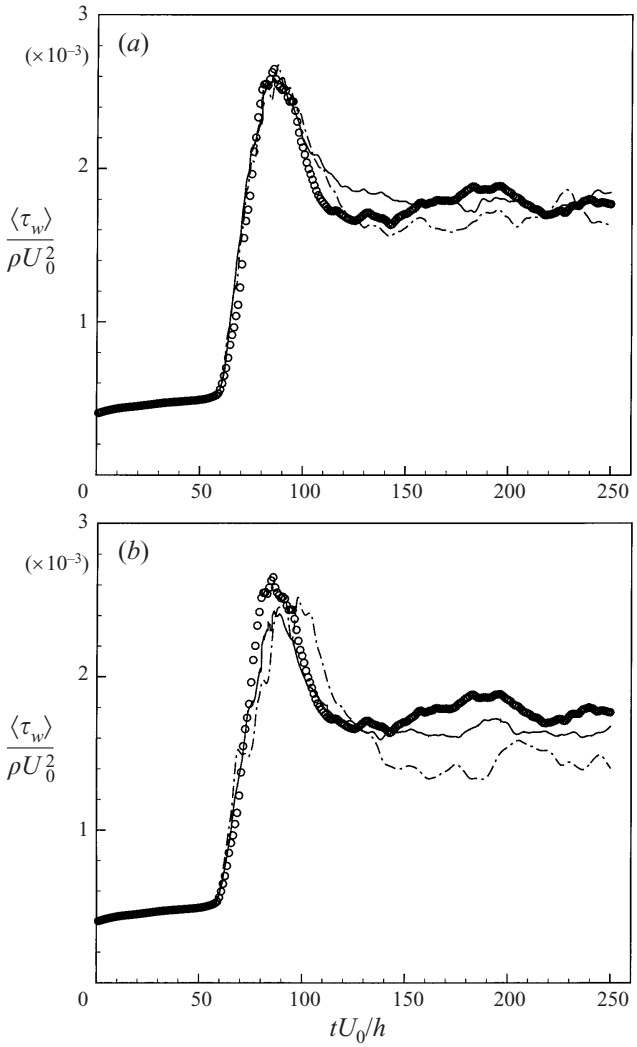


FIGURE 19. Time evolution of the mean wall-shear stress in the transitional and turbulent channel flow predicted by (*a*) resolved LES, and (*b*) coarse LES compared to DNS: ○, DNS; ——, DTM; — · —, DSM.

7.2. *LES of transitional and turbulent channel flow*

As a second test case, we evaluate the performance of DTM in LES of a transitional and turbulent channel flow. The channel is assumed to be periodic in the streamwise (x) and spanwise (y) directions with periodicity lengths of $L_x = L_y = 2\pi h/\alpha = 2\pi h/\beta$, where h denotes the channel half-width and $\alpha = \beta = 1.25$. The simulations were performed using the pseudo-spectral methods described in § 7.1 and imposed a constant flow rate in the channel. The Reynolds number of the flow based on bulk velocity and channel half-width was $Re_m = U_m h/\nu = 3300$, which corresponds to a $Re_\tau = u_\tau h/\nu \sim 210$ in the fully developed turbulent channel. The performance of DTM was evaluated through comparisons with results from DSM and DNS. The DNS of channel flow was performed with a resolution of $64 \times 128 \times 129$, resulting in grid spacings of $\Delta_x^+ \approx 16$, $\Delta_y^+ \approx 8$, and $0.065 < \Delta_z^+ < 5.2$ in the turbulent channel. The LES were performed at two resolutions, $16 \times 64 \times 65$ and $16 \times 32 \times 65$. The lower

https://doi.org/10.1017/S0022112099007582 Published online by Cambridge University Press

			Resolved LES		Coarse LES	
	DNS	Dean	DTM	DSM	DTM	DSM
$C_f \times 10^3$	8.08	8.08	8.00	7.57	7.43	6.49
U_c/U_m	1.17	1.16	1.16	1.15	1.17	1.19

TABLE 1. The friction coefficient C_f and centreline to bulk velocity ratio U_c/U_m predicted by LES compared to DNS and Dean's correlation.

resolution run was performed to evaluate the degradation of the results at marginal LES resolutions. Both the DNS and the LES runs were de-aliased in the homogeneous directions using the 2/3 rule. Filtering was performed using sharp (Fourier) filters and was applied only in the homogeneous (x and y) directions. In the well-resolved LES, the filters $\overline{k_i}/\widetilde{k_i}/\widehat{k_i}$ were placed at 5/4/3 in the x-direction, and 20/16/10 in the y-direction. In the coarse LES, these filters were placed at 5/4/3 and 10/8/5 in the x- and y-directions, respectively. The effective resolution in LES was $\overline{\Delta}_x^{\,+} \approx 100$, and $\overline{\Delta}_y^{\,+} \approx 25$ in the well-resolved computations, and $\overline{\Delta}_x^{\,+} \approx 100$, and $\overline{\Delta}_y^{\,+} \approx 50$ in the coarse computations. Both the DNS and LES runs were started from laminar flow on which a combination of two- and three-dimensional least-stable eigenmodes of the Orr–Sommerfeld equation were superimposed.

The time evolution of the mean wall-shear stress in the channel predicted by LES is compared to DNS results in figure 19. The wall-shear stress remains nearly constant for $tU_0/h < 50$ when the disturbance field is still infinitesimal, experiences a rapid rise during the transition period $60 < tU_0/h < 85$, reaches its peak at $tU_0/h \sim 85$, and eventually equilibrates to a fully developed turbulent state for $tU_0/h > 120$. The average (averaged over $160 \leqslant tU_o/h \leqslant 250$) skin-friction coefficient, $C_f = \langle \tau_w \rangle / \frac{1}{2}\rho U_m^2$, and the ratio, U_c/U_m, of the mean centreline velocity to the bulk velocity in the fully developed turbulent channel are compared to results from DNS and Dean's correlation in table 1. With DTM, the predicted friction coefficient and centreline velocity are within 1% of the DNS results in the well-resolved computations, and within 8% of the DNS results in the coarse LES. With DSM, the friction coefficient is under-predicted by 6% in the well-resolved computations, and by 20% in the coarse LES. The onset of transition and the peak of the wall-shear stress are accurately predicted by both models in the well-resolved computations. In the coarse LES, both models under-predict the magnitude of this peak and its occurrence is delayed when DSM is used as the model.

Figure 20 shows the mean turbulence statistics in the fully developed turbulent channel compared to the DNS data filtered at the same conditions as those used in LES. For reference, the unfiltered DNS data are also shown. With DTM, the predicted mean velocity and turbulence intensities are in agreement with the filtered DNS data in the well-resolved computations (figure 20*a*, *b*). DSM fails to produce a logarithmic layer with a constant slope in the mean velocity, over-predicts the magnitude of the streamwise turbulence intensity, and places the peak of the streamwise turbulence intensity further away from the wall than in DNS. At marginal resolutions (figure 20*c*, *d*), the LES predictions become less accurate with both models. However, the DTM predictions remain reasonably accurate, while those from DSM markedly deteriorate.

The near-wall flow structure obtained in the well-resolved LES is compared to DNS results in figure 21. The near-wall structure is examined through the two-point correlations of the streamwise velocity fluctuations at $z^+ = 10$ for points separated in

https://doi.org/10.1017/S0022112099007582 Published online by Cambridge University Press

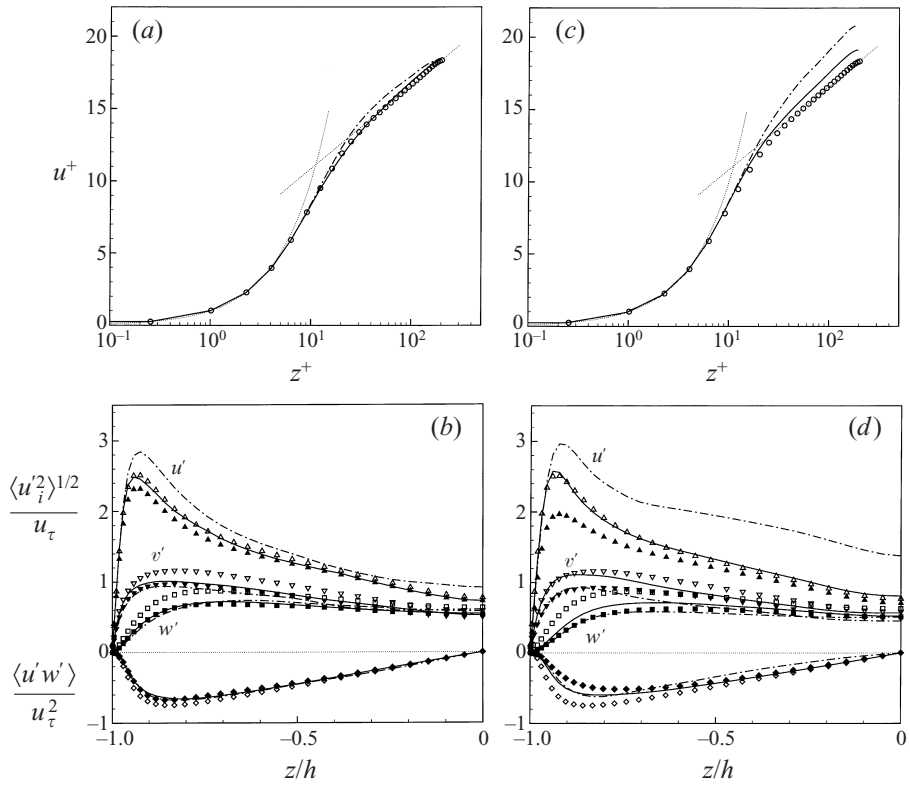


FIGURE 20. Mean turbulence statistics in the fully developed turbulent channel predicted in (a,b) resolved LES, and (c,d) coarse LES, compared to DNS. ——, DTM; — · —, DSM; open symbols, DNS; filled symbols, filtered DNS: ○, mean velocity; △, u_{rms}; ▽, v_{rms}; □, w_{rms}; ◇, resolved shear stress.

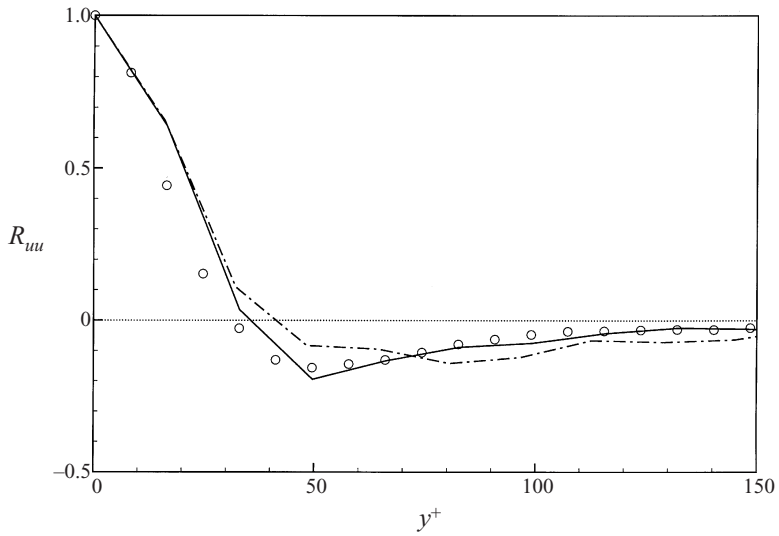


FIGURE 21. Spanwise two-point correlation of the streamwise fluctuating velocity in the fully developed turbulent channel at $z^+ = 10$ predicted by LES compared to DNS: ○, DNS; ——, DTM; — · —, DSM.

https://doi.org/10.1017/S0022112099007582 Published online by Cambridge University Press

the spanwise direction. The location of the minimum in this correlation denotes half of the mean spacing between the high- and low-speed streaks in the wall layer. With DTM, the predicted mean streak spacing is ~ 100 wall-units, in agreement with DNS and known experimental results. In contrast, DSM predicts a mean streak spacing ~ 160 wall units.

Overall, these results demonstrate the ability of DTM to accurately predict the mean statistics, spectra, and structure in LES without excessive resolution requirements.

8. Extension to graded filters

In §§ 5–7, the two-component parameterization (5.1) was developed and tested for sharp (Fourier) filters. Sharp filters do not provide an overlap between the resolved and subgrid scales of motion. Consequently, the local-interactions term, τ'_{ij}, in the two-component parameterization (5.1) had to be approximated by that at a neighbouring cutoff within the resolved scales. This is not necessary with graded filters, which provide an overlap between the resolved and subgrid scales. In this section, we discuss the extension of the two-component parameterization (5.1) to graded filters.

For graded filters, the true SGS stress is given by

$$\tau_{ij} = \eta_{ij} - L_{ij} = (\overline{u_i u_j} - \overline{u}_i \overline{u}_j) - (\overline{\overline{u}_i \overline{u}_j} - \overline{\overline{u}}_i \overline{\overline{u}}_j), \tag{8.1}$$

where the overbar denotes a graded LES filter of characteristic scale $\overline{k}$ in the wavenumber space. The true SGS stress arising from local interactions between the resolved and subgrid scales near the LES filter is, by analogy with (5.2), given by

$$\tau'_{ij} = \tau^t_{ij} = \eta^t_{ij} - L^t_{ij} = (\overline{\breve{u}_i \breve{u}_j} - \overline{\breve{u}}_i \overline{\breve{u}}_j) - (\overline{\overline{\breve{u}}_i \overline{\breve{u}}_j} - \overline{\overline{\breve{u}}}_i \overline{\overline{\breve{u}}}_j), \tag{8.2}$$

where $\breve{u}_i$ represents the velocity field truncated to (i.e. filtered with a *sharp* filter at) $k_t \gtrsim \overline{k}$. Substituting (8.1) and (8.2) into (5.1), approximating $L^t_{ij} \approx L_{ij}$, and using a Smagorinsky parameterization for the eddy-viscosity term gives the formulation of the two-component model for graded filters as

$$\eta^*_{ij} = -2C\overline{\Delta}^2 |\overline{S}| \overline{S}_{ij} + (\overline{\breve{u}_i \breve{u}_j} - \overline{\breve{u}}_i \overline{\breve{u}}_j)^*. \tag{8.3}$$

This formulation is readily available in pseudo-spectral computations, where $\breve{u}_i$ can easily be recovered from the quantity computed at the grid scale.

The major difference between this parameterization and classical mixed models is in the formulation of the local-interactions term. In traditional mixed formulations, the local interactions are computed based on a similarity argument as $C_L(\overline{\overline{u}_i \overline{u}_j} - \overline{\overline{u}}_i \overline{\overline{u}}_j)$ (Bardina *et al.* 1980; Zang *et al.* 1993; Salvetti & Banerjee 1995) or as $C_L(\widetilde{\overline{u}_i \overline{u}_j} - \widetilde{\overline{u}}_i \widetilde{\overline{u}}_j)$ (Liu *et al.* 1994), where the tilde represents a graded filter similar in shape but of a larger width (typically $2\overline{\Delta}$). With $C_L = 1$ this term represents the nonlinear interactions between the scales represented in $\overline{\overline{u}}_i$ (or $\widetilde{\overline{u}}_i$) and those between $\overline{\overline{u}}_i$ and $\overline{u}_i$ (or between $\widetilde{\overline{u}}_i$ and $\overline{u}_i$). This provides only a partial representation of the local interactions. As a result, when C_L is left as an undetermined model coefficient (Salvetti & Banerjee 1995), dynamic procedures predict the optimal value of C_L to be higher than 1 (around 1.4 for a box filter). However, even with C_L computed dynamically, such a similarity term can provide only a partial representation of the local interactions. Recovering the full local interactions from the similarity term requires an appropriate weighting (depending on the shape of the filter) of the different wavenumbers in the overlap zone between the resolved and subgrid scales. Alternatively, one can directly obtain the local interactions based on (8.3) using dissimilar filters (one sharp, one

https://doi.org/10.1017/S0022112099007582 Published online by Cambridge University Press

graded). Preliminary applications of (8.3) in LES show this formulation to be superior to existing mixed models. These results will be reported in a future communication.

9. Summary and conclusions

The dynamics of subgrid-scale energy transfer in turbulent shear flows has been investigated using a DNS database of a temporally growing, planar turbulent jet at $Re_\lambda \approx 110$. In agreement with earlier analytical predictions (Kraichnan 1976), we find subgrid-scale energy transfer to arise from two distinct effects: one representing non-local transfers of energy from the resolved scales to disparate subgrid scales, the other representing local two-way exchanges of energy between the resolved scales and subgrid wavenumbers near the cutoff. In the physical space, the former is manifested as low-intensity, forward transfers of energy; the latter gives rise to intense and coherent regions of forward and reverse transfer, of scale comparable to the size of the LES cutoff, which are spatially correlated with the organized vortical structures at that scale. The local interactions arise primarily from a very narrow band of subgrid wavenumbers between k_m and $1.25k_m$, not the whole octave between k_m and $2k_m$ as previously suggested. This opens up new possibilities for modelling these interactions.

A dynamic two-component model (DTM), incorporating these effects is developed for sharp (Fourier) filters. In this model, the non-local forward transfers of energy are parameterized using an eddy-viscosity term, while the local interactions are modelled based on the dynamics of the resolved scales near the LES cutoff. This model offers many advantages over pure eddy-viscosity parameterizations. In particular, the model is inherently local and accounts for backscatter based on the dynamics of the resolved scales. *A priori* tests of the model show that it predicts the mean subgrid-scale dissipation and the mean subgrid-scale stresses in better agreement with DNS results than dynamic eddy-viscosity models. In addition, the model correctly predicts the breakdown of the net transfer into forward and reverse contributions and gives a local structure of the subgrid-scale dissipation field in general agreement with DNS. The inclusion of the local-interactions term results in a much narrower distribution of model-coefficient values compared to pure eddy-viscosity models. This eliminates the need for averaging the model coefficient, making the model inherently local and thus suitable for application to LES of complex-geometry flows. In applications to LES of transitional and turbulent jet and channel flows, DTM predicts the statistics, structure and spectra in better agreement with DNS results than the dynamic Smagorinsky model (DSM). In addition, the model remains robust at marginal resolutions.

Extension of the model to graded filters suggests a different construction of the local-interactions term than that used in existing mixed models based on similarity arguments.

This work was supported by AFOSR contract AFOSR-91-0402, and in part by ONR contract N00014-92-J-1750, and NSF contract ASC-94-05085. The computations were performed at the San Diego Supercomputer Center and the Center for Parallel Computing at the University of Michigan. This support is gratefully acknowledged. We are also grateful to Dr Martin Prince for review of the manuscript and helpful comments.

Appendix A. Subgrid-scale transfer in the spectral space

In analysing the dynamics of subgrid-scale energy transfer in the spectral space, we consider the energetics of the turbulent velocity fluctuations separate from that

https://doi.org/10.1017/S0022112099007582 Published online by Cambridge University Press

of the mean flow. This is done in order to preserve certain conservation properties and to allow comparisons with analytical results derived for isotropic turbulence. The equation governing the dynamics of the fluctuating velocity u'_α is given by (Hinze 1975),

$$\left(\frac{\partial}{\partial t} - \nu\nabla^2\right) u'_\alpha(\boldsymbol{x},t) = -N'_\alpha(\boldsymbol{x},t) - N'^{\mathscr{M}}_\alpha(\boldsymbol{x},t), \tag{A 1}$$

where

$$N'_\alpha(\boldsymbol{x},t) = \frac{\partial}{\partial x_\beta}(u'_\alpha u'_\beta) + \frac{1}{\rho}\frac{\partial p''}{\partial x_\alpha} \tag{A 2}$$

with

$$\frac{1}{\rho}\frac{\partial^2 p''}{\partial x_\alpha \partial x_\alpha} = -\frac{\partial^2}{\partial x_\alpha \partial x_\beta}(u'_\alpha u'_\beta)$$

represents the mutual nonlinear interactions between the turbulent velocity fluctuations, and

$$N'^{\mathscr{M}}_\alpha(\boldsymbol{x},t) = u'_3\frac{\partial U}{\partial x_3}\delta_{\alpha 1} + U\frac{\partial u'_\alpha}{\partial x_1} + \frac{\partial}{\partial x_3}(\langle u'_\alpha u'_3\rangle) + \frac{1}{\rho}\frac{\partial p'^{\mathscr{M}}}{\partial x_\alpha} \tag{A 3}$$

with

$$\frac{1}{\rho}\frac{\partial^2 p'^{\mathscr{M}}}{\partial x_\alpha \partial x_\alpha} = -2\frac{\partial u'_3}{\partial x_1}\frac{\partial U}{\partial x_3} + \frac{\partial^2}{\partial x_\alpha \partial x_3}(\langle u'_\alpha u'_3\rangle)$$

represents the nonlinear interactions of the fluctuating velocity with the mean flow. The governing equation for the large-scale fluctuating velocity $u'^{\mathscr{L}}_\alpha(\boldsymbol{x},t)$ can be obtained by a truncation of the equation (A 1) to the large scales

$$\left(\frac{\partial}{\partial t} - \nu\nabla^2\right) u'^{\mathscr{L}}_\alpha(\boldsymbol{x},t) = -N'^{\mathscr{L}|\mathscr{L}}_\alpha(\boldsymbol{x},t) - N'^{\mathscr{L}|\mathscr{S}}_\alpha(\boldsymbol{x},t) - N'^{\mathscr{M}\mathscr{L}}_\alpha(\boldsymbol{x},t), \tag{A 4}$$

where

$$N'^{\mathscr{L}|\mathscr{L}}_\alpha(\boldsymbol{x},t) = \frac{\partial}{\partial x_\beta}(u'^{\mathscr{L}}_\alpha u'^{\mathscr{L}}_\beta)^{\mathscr{L}} + \frac{1}{\rho}\frac{\partial}{\partial x_\alpha}p''^{\mathscr{L}|\mathscr{L}} \tag{A 5}$$

with

$$\frac{1}{\rho}\frac{\partial^2 p''^{\mathscr{L}|\mathscr{L}}}{\partial x_\alpha \partial x_\alpha} = -\frac{\partial^2}{\partial x_\alpha \partial x_\beta}(u'^{\mathscr{L}}_\alpha u'^{\mathscr{L}}_\beta)^{\mathscr{L}}$$

represents the large-scale nonlinear interactions between the large-scale velocity fluctuations,

$$N'^{\mathscr{L}|\mathscr{S}}_\alpha(\boldsymbol{x},t) = \frac{\partial}{\partial x_\beta}(u'_\alpha u'_\beta - u'^{\mathscr{L}}_\alpha u'^{\mathscr{L}}_\beta)^{\mathscr{L}} + \frac{1}{\rho}\frac{\partial}{\partial x_\alpha}p''^{\mathscr{L}|\mathscr{S}} \tag{A 6}$$

with

$$\frac{1}{\rho}\frac{\partial^2 p''^{\mathscr{L}|\mathscr{S}}}{\partial x_\alpha \partial x_\alpha} = -\frac{\partial^2}{\partial x_\alpha \partial x_\beta}(u'_\alpha u'_\beta - u'^{\mathscr{L}}_\alpha u'^{\mathscr{L}}_\beta)^{\mathscr{L}}$$

represents the large-scale nonlinear interactions of the large-scale fluctuating velocity field with the subgrid scales, and $N'^{\mathscr{M}\mathscr{L}}_\alpha(\boldsymbol{x},t)$ represents the large-scale nonlinear interactions of the large-scale fluctuating velocity field with the mean flow.

The subgrid-scale transfer of energy $T_S(k|k_m)$ to a resolved scale k due to nonlinear interactions with the subgrid scales can be obtained from (A 4) by considering the evolution equation for kinetic energy of the large-scale turbulent velocity fluctuations

https://doi.org/10.1017/S0022112099007582 Published online by Cambridge University Press

in the wavenumber space

$$\left(\frac{\partial}{\partial t}+2\nu k^2\right)E^{\mathscr{L}}(k,t)=T_L(k|k_m,t)+T_S(k|k_m,t)+T^{\mathscr{M}\mathscr{L}}(k|k_m,t), \tag{A 7}$$

where

$$T_L(k|k_m,t)=-\sum_{k-\frac{1}{2}<|\boldsymbol{k}|\leqslant k+\frac{1}{2}}\mathrm{Re}\left\{\check{u}'^{*\mathscr{L}}_{\alpha}(\boldsymbol{k},t)\check{N}'^{\mathscr{L}|\mathscr{L}}_{\alpha}(\boldsymbol{k},t)\right\} \tag{A 8}$$

represents the transfer of energy to the scale k as a result of mutual interactions between the large-scale velocity fluctuations,

$$T_S(k|k_m,t)=-\sum_{k-\frac{1}{2}<|\boldsymbol{k}|\leqslant k+\frac{1}{2}}\mathrm{Re}\left\{\check{u}'^{*\mathscr{L}}_{\alpha}(\boldsymbol{k},t)\check{N}'^{\mathscr{L}|\mathscr{S}}_{\alpha}(\boldsymbol{k},t)\right\} \tag{A 9}$$

represents the transfer of energy to the scale k as a result of interactions with the subgrid-scale velocity fluctuations, $T^{\mathscr{M}\mathscr{L}}(k|k_m,t)$ represents the transfer of energy to the scale k as a result of interactions with the mean flow and $\check{}$ and * denote Fourier transform and complex conjugate, respectively.

An analogous quantity, $t_s^{(n|m)}[\boldsymbol{i}]$, representing the transfer of energy to a resolved scale n (corresponding to all modes with wavenumber $k-\frac{1}{2}\Delta k<|\boldsymbol{k}|\leqslant k+\frac{1}{2}\Delta k$, with $k=2\pi/2^n h$ and $\Delta k=k\ln 2$) at location $2^n h\boldsymbol{i}$ due to dynamical interactions with the subgrid scales (all modes with wavenumber $|\boldsymbol{k}|>k_m=2\pi/2^m h$) can also be defined using the wavelet analysis as

$$t_s^{(n|m)}[\boldsymbol{i}]=-\sum_{q=1}^{7}u'^{\mathscr{L}(n,q)}_{\alpha}[\boldsymbol{i}]N'^{\mathscr{L}|\mathscr{S}(n,q)}_{\alpha}[\boldsymbol{i}], \tag{A 10}$$

where $u'^{\mathscr{L}(n,q)}_{\alpha}$ is the wavelet transform of the large-scale disturbance velocity and $N'^{\mathscr{L}|\mathscr{S}(n,q)}_{\alpha}[\boldsymbol{i}]$ is the wavelet transform of the nonlinear term given by equation (A 6). Note that, for consistency of results, the resolved and subgrid scales are defined using a sharp (Fourier) filter even when a wavelet analysis is used.

Appendix B. Subgrid-scale transfer in the physical space

In analysing the dynamics of subgrid-scale energy transfer in the physical space, we do not separate the energetics of the large-scale turbulent velocity fluctuations from that of the mean flow. This is done in order to remain consistent with the formulation of LES equations in the physical space, in which the subgrid-scale stresses represent the effect of the subgrid scales on the full resolved-scale flow field. The equation governing the dynamics of the large-scale flow field in the physical space is given by the filtered Navier–Stokes equations

$$\left(\frac{\partial}{\partial t}-\nu\nabla^2\right)u^{\mathscr{L}}_{\alpha}(\boldsymbol{x},t)=-N^{\mathscr{L}|\mathscr{L}}_{\alpha}(\boldsymbol{x},t)-N^{\mathscr{L}|\mathscr{S}}_{\alpha}(\boldsymbol{x},t), \tag{B 1}$$

where $u^{\mathscr{L}}_{\alpha}(\boldsymbol{x},t)$ is the resolved-scale velocity,

$$N^{\mathscr{L}|\mathscr{L}}_{\alpha}(\boldsymbol{x},t)=\frac{\partial}{\partial x_\beta}(u^{\mathscr{L}}_{\alpha}u^{\mathscr{L}}_{\beta})^{\mathscr{L}}-\frac{1}{\rho}\frac{\partial p^{\mathscr{L}|\mathscr{L}}}{\partial x_\alpha} \tag{B 2}$$

https://doi.org/10.1017/S0022112099007582 Published online by Cambridge University Press

with

$$\frac{1}{\rho}\frac{\partial^2 p^{\mathscr{L}|\mathscr{L}}}{\partial x_\alpha \partial x_\alpha} = -\frac{\partial^2}{\partial x_\alpha \partial x_\beta}(u_\alpha u_\beta)^{\mathscr{L}}$$

represents the large-scale mutual nonlinear interactions of the resolved scales, and

$$N_\alpha^{\mathscr{L}|\mathscr{S}}(\boldsymbol{x},t) = \frac{\partial}{\partial x_\beta}(u_\alpha u_\beta - u_\alpha^{\mathscr{L}} u_\beta^{\mathscr{L}})^{\mathscr{L}} + \frac{1}{\rho}\frac{\partial}{\partial x_\alpha} p^{\mathscr{L}|\mathscr{S}} \tag{B 3}$$

with

$$\frac{1}{\rho}\frac{\partial^2 p^{\mathscr{L}|\mathscr{S}}}{\partial x_\alpha \partial x_\alpha} = -\frac{\partial^2}{\partial x_\alpha \partial x_\beta}(u_\alpha u_\beta - u_\alpha^{\mathscr{L}} u_\beta^{\mathscr{L}})^{\mathscr{L}}$$

represents the large-scale nonlinear interactions of the resolved flow with the subgrid scales.

The equation governing the energetics of the resolved-scale velocity field in the physical space can then be obtained from equation (B 1) by considering the evolution of the kinetic energy of the resolved scales

$$\frac{\partial}{\partial t}\left(\frac{u_\alpha^{\mathscr{L}}(\boldsymbol{x},t)}{2}\right)^2 = T_L(\boldsymbol{x},t) + T_S(\boldsymbol{x},t) + \nu u_\alpha^{\mathscr{L}} \nabla^2 u_\alpha^{\mathscr{L}}, \tag{B 4}$$

where

$$T_L(\boldsymbol{x},t) = -u_\alpha^{\mathscr{L}}(\boldsymbol{x},t) N_\alpha^{\mathscr{L}|\mathscr{L}}(\boldsymbol{x},t) \tag{B 5}$$

represents transfer of energy to the large scales due to mutual nonlinear interactions between the resolved scales, and

$$T_S(\boldsymbol{x},t) = -u_\alpha^{\mathscr{L}}(\boldsymbol{x},t) N_\alpha^{\mathscr{L}|\mathscr{S}}(\boldsymbol{x},t) \tag{B 6}$$

represents the transfer of energy to the large scales due to nonlinear interactions with the subgrid scales. The quantity $T_S(\boldsymbol{x},t)$ given by equation (B 6) represents the total transfer of energy in the physical space due to interactions with the subgrid scales. Using equations (B 6) and (B 3), $T_S(\boldsymbol{x},t)$ can be broken down into a sum of two redistribution terms (with zero global mean) plus a true drain term, representing the dissipation of large-scale kinetic energy due to subgrid-scale interactions,

$$T_S(\boldsymbol{x},t) = -\frac{\partial}{\partial x_\beta}(u_\alpha^{\mathscr{L}} \tau_{\alpha\beta}) - \frac{\partial}{\partial x_\alpha}(u_\alpha^{\mathscr{L}} p^{\mathscr{L}|\mathscr{S}}) - \epsilon_S(\boldsymbol{x},t) \tag{B 7}$$

where

$$\epsilon_S(\boldsymbol{x},t) = -\tau_{\alpha\beta} S_{\alpha\beta}^{\mathscr{L}} \tag{B 8}$$

represents the subgrid-scale dissipation, and $\tau_{\alpha\beta}(\boldsymbol{x},t) = (u_\alpha u_\beta - u_\alpha^{\mathscr{L}} u_\beta^{\mathscr{L}})^{\mathscr{L}}$ and

$$S_{\alpha\beta}^{\mathscr{L}} = \frac{1}{2}\left(\frac{\partial u_\alpha^{\mathscr{L}}}{\partial x_\beta} + \frac{\partial u_\beta^{\mathscr{L}}}{\partial x_\alpha}\right)$$

represent the subgrid-scale stress and the large-scale strain rate tensors, respectively. In considering the dynamics of subgrid-scale energy transfer in the physical space, it is customary to neglect the redistribution terms and consider only the dynamics of subgrid-scale dissipation. In keeping with this tradition, we have also based our discussion of subgrid-scale energy transfer in the physical space on the subgrid-scale dissipation $\epsilon_S(\boldsymbol{x},t)$ instead of the total transfer $T_S(\boldsymbol{x},t)$.

https://doi.org/10.1017/S0022112099007582 Published online by Cambridge University Press

REFERENCES

Ansari, A. 1993 Small-scale dynamics and subgrid interactions in turbulent shear flows. Doctoral thesis, The University of Michigan.

Anselmet, F., Gagne, Y., Hopfinger, E. J. & Antonia, R. A. 1984 Higher order velocity structure functions in turbulent shear flows. *J. Fluid Mech.* **140**, 63–89.

Bardina, J., Ferziger, J. H. & Reynolds, W. C. 1980 Improved subgrid scale models for large eddy simulation. *AIAA 13th Fluid & Plasma Dynamics Conference, Colorado.*

Bertoglio, J. P. 1985 A stochastic-grid model for sheared turbulence. In *Macroscopic Modelling of Turbulent Flows* (ed. U. Frisch, J. B. Keller, G. Papanicolaou & O. Pironneau), pp. 100–119. Springer.

Carati, D., Ghosal, S. & Moin, P. 1995 On the representation of backscatter in dynamic localization models. *Phys. Fluids* **3**, 606–616.

Chasnov, J. R. 1991 Simulation of the Kolmogorov inertial subrange using an improved subgrid model. *Phys. Fluids* A **3**, 188–200.

Chollet, J. P. & Lesieur, M. 1981 Parameterization of small scales of three-dimensional isotropic turbulence utilizing spectral closures. *J. Atmos. Sci.* **38**, 2747–2757.

Clark, R. A., Ferziger, J. H. & Reynolds, W. C. 1979 Evaluation of subgrid–scale models using an accurately simulated turbulent flow. *J. Fluid Mech.* **91**, 1–16.

Daubechies, I. 1988 Orthonormal bases of compactly supported wavelets. *Commun. Pure Appl. Maths* **41**, 909–996.

Domaradzki, J. A. 1992 Nonlocal triad interactions and the dissipation range of isotropic turbulence. *Phys. Fluids* A **4**, 2037–2045.

Domaradzki, J. A., Liu, W. & Brachet, M. E. 1993 An analysis subgrid-scale interactions in numerically simulated isotropic turbulence. *Phys. Fluids* A **5**, 1747–1759.

Domaradzki, A., Liu, W., Hartel, C. & Kleiser, L. 1994 Energy transfer in numerically simulated wall-bounded turbulent flows. *Phys. Fluids* A **4**, 1583–1599.

Domaradzki, A., Metcalfe, R. S., Rogallo, R. S. & Riley, J. J. 1987 Analysis of subgrid-scale eddy viscosity with the use of results from direct numerical simulations. *Phys. Rev. Lett.* **58**, 547–550.

Domaradzki, A. & Rogallo, R. S. 1990 Local energy transfer and nonlocal interactions in homogeneous, isotropic turbulence. *Phys. Fluids* A **2**, 413–426.

Domaradzki, J. A. & Saiki, E. M. 1997 A subgrid-scale model based on the estimation of unresolved scales of turbulence. *Phys. Fluids* **9**, 2148–2164.

Farge, M. 1992 Wavelet transforms and their application to turbulence. *Ann. Rev. Fluid Mech.* **24**, 395–457.

Farge, M., Kevlahan, N., Perrier, V. & Goirand, E. 1996 Wavelets and turbulence. *Proc. IEEE* **84**, 639–669.

Frisch, U., Sulem, P. & Nelkin, M. 1978 A simple dynamical model of intermittent fully developed turbulence. *J. Fluid Mech.* **87**, 719–736.

Galperin, B. & Orszag, S. A. 1993 *Large-Eddy Simulation of Complex Engineering and Geophysical Flows.* Cambridge University Press.

Germano, M. 1986 A proposal for a redefinition of the turbulent stresses in the filtered Navier–Stokes equations. *Phys. Fluids* **29**, 2323–2324.

Germano, M., Piomelli, U., Moin, P. & Cabot, W. H. 1991 A dynamic subgrid-scale eddy viscosity model. *Phys. Fluids* A **3**, 1760–1765.

Ghosal, S. G., Lund, T. S., Moin, P. & Akselvoll, K. 1995 A dynamic localization model for large-eddy simulation of turbulent flows. *J. Fluid Mech.* **286**, 229–255.

Hinze, J. O. 1975 *Turbulence* McGraw-Hill.

Horiuti, K. 1989 The role of the Bardina model in large eddy simulation of turbulent channel flow. *Phys. Fluids* A **1**, 426–428.

Horiuti, K. 1993 A proper velocity scale for modeling subgrid-scale viscosities in large eddy simulation. *Phys. Fluids* A **5**, 146–157.

Horiuti, K. 1997 A new dynamic two-parameter mixed model for large-eddy simulation *Phys. Fluids* A **9**, 3443–3464.

Kida, S. & Murakami, Y. 1987 Kolmogorov similarity in freely decaying turbulence. *Phys. Fluids* **30**, 2030–2039.

https://doi.org/10.1017/S0022112099007582 Published online by Cambridge University Press

KOLMOGOROV, A. N. 1941 The local structure of turbulence in incompressible viscous fluid for very large Reynolds numbers. *C. R. Acad. Sci. USSR* **30**, 301–305.

KOLMOGOROV, A. N. 1961 A refinement of previous hypotheses concerning the local structure of turbulence in a viscous incompressible fluid at high Reynolds number. *J. Fluid Mech.* **13**, 82–85.

KRAICHNAN, R. H. 1976 Eddy viscosity in two and three dimensions. *J. Atmos. Sci.* **33**, 1521–1536.

KWAK, D., REYNOLDS, W. C. & FERZIGER, J. H. 1975 Three dimensional time dependent computation of turbulent flows. *Mech. Engng Dept. Stanford Univ. Rep.* TF-5.

LEITH, C. E. 1990 Stochastic backscatter in a subgrid-scale model: Plane shear mixing layer. *Phys. Fluids* A **2**, 297–299.

LEONARD, A. 1974 Energy cascade in large-eddy simulations of turbulent fluid flows. *Adv. Geophys.* A **18**, 237–248.

LESIEUR, M. 1991 *Turbulence in Fluids*. Kluwer.

LESIEUR, M. & METAIS, O. 1996 New trends in large-eddy simulations of turbulence. *Ann. Rev. Fluid Mech.* **28**, 45–82.

LESLIE, D. C. & QUARINI, G. L. 1979 The application of turbulence theory to the formulation of subgrid modelling procedures. *J. Fluid Mech.* **91**, 65–91.

LILLY, D. K. 1967 The presentation of small-scale turbulence in numerical simulation experiments. *Proc. IBM Sci. Comput. Symp. on Environmental Sci.*, pp. 195–210.

LILLY, D. K. 1992 A proposed modification of the Germano subgrid-scale closure method. *Phys. Fluids* A **4**, 633–635.

LIU, S., MENEVEAU, C. & KATZ, J. 1994 On the properties of similarity subgrid-scale models as deduced from measurements in a turbulent jet. *J. Fluid Mech.* **275**, 83–119.

LUND, T. S., GHOSAL, S. & MOIN, P. 1993 Numerical experiments with highly variable eddy viscosity models. In *Engineering applications of Large Eddy Simulations* (ed. S. A. Ragale & U. Piomelli). ASME FED, vol. 162, pp. 7–11.

MALLAT, S. G. 1989 A theory for multi-resolution signal decomposition: The wavelet representation. *IEEE Trans. Pattern Anal. Mach. Int.* **11**, 674–693.

MASON, P. J. & THOMSON, D. J. 1992 Stochastic backscatter in large-eddy simulations of boundary layers. *J. Fluid Mech.* **242**, 51–78.

MENEVEAU, C. 1991 Analysis of turbulence in the orthonormal wavelet representation. *J. Fluid Mech.* **232**, 469–520.

MENEVEAU, C., LUND, T. S. & CABOT, W. H. 1996 A Lagrangian dynamic subgrid-scale model of turbulence. *J. Fluid Mech.* **319**, 353–385.

METAIS, O. & FERZIGER, J. 1997 *New Tools in Turbulence Modelling*. Springer.

METAIS, O. & LESIEUR, M. 1992 Spectral large-eddy simulation of isotropic and stably stratified turbulence. *J. Fluid Mech.* **23**, 157–194.

MONIN, A. S. & YAGLOM, A. M. 1981 *Statistical Fluid Mechanics II*. MIT Press.

O'NEIL, J. & MENEVEAU, C. 1997 Subgrid-scale stresses and their modelling in a turbulent plane wake. *J. Fluid Mech.* **349**, 253–293.

OHKITANI, K. & KIDA, S. 1992 Triad interactions in a forced turbulence. *Phys. Fluids* A **4**, 794–802.

PAO, Y. H. 1965 Structure of turbulent velocity and scalar fields at large wavenumbers. *Phys. Fluids* **8**, 1063–1075.

PIOMELLI, U., CABOT, W. H., MOIN, P. & LEE, S. 1991 Subgrid-scale backscatter in turbulent and transitional flows. *Phys. Fluids* A **3**, 1766–1771.

PIOMELLI, U. & LIU, J. 1995 Large-eddy simulation of rotating channel flows using a localized dynamic model. *Phys. Fluids* A **7**, 839–848.

PIOMELLI, U., YU, Y. & ADRIAN, R. 1996 Subgrid-scale energy transfer and near-wall turbulence structure. *Phys. Fluids* **8**, 215–224.

ROGALLO, R. & MOIN, P. 1984 Numerical simulation of turbulent flows. *Ann. Rev. Fluid Mech.* **16**, 99–137.

SALVETTI, M. V. & BANERJEE, S. 1995 A priori tests of a new dynamic subgrid-scale model for finite-difference large-eddy simulations. *Phys. Fluids* A **7**, 2831–2847.

SHAH, K. B. & FERZIGER, J. H. 1995 A new non-eddy viscosity subgrid-scale model and its application to channel flow. *Center for Turbulence Research Ann. Res. Briefs*, pp. 73–90.

https://doi.org/10.1017/S0022112099007582 Published online by Cambridge University Press

Schumann, U. 1975 Subgrid scale model for finite difference simulations of turbulent flows in plane channels and annuli. *J. Comput. Phys.* **18**, 376–404.

Schumann, U. 1995 Stochastic backscatter of turbulence energy and scalar variance by random subgrid-scale fluxes. *Proc. R. Soc. Lond.* A **451**, 193–318.

Smagorinsky, J. 1963 General circulation experiments with the primitive equations. *Mon. Weath. Rev.* **91**, 99–164.

Tennekes, H. & Lumley, J. L. 1972 *A First Course in Turbulence*. MIT Press.

Townsend, A. A. 1949 The fully developed turbulent wake of a circular cylinder. *Austral. J. Sci. Res.* **2**, 451–468.

Vincent, A. & Meneguzzi, M. 1991 The spatial structure and statistical properties of homogeneous turbulence. *J. Fluid Mech.* **225**, 1–20.

Waleffe, F. 1992 The nature of triad interactions in homogeneous turbulence. *Phys. Fluids* A **4**, 350–363.

Yakhot, A., Orszag, S. A., Yakhot, V. & Israeli, M. 1989 Renormalization group formulation of large-eddy simulations. *J. Sci. Comput.* **4**, 139–158.

Zang, Y., Street, R. L. & Koseff, J. R. 1993 A dynamic mixed subgrid-scale model and its application to turbulent recirculating flows. *Phys. Fluids* A **5**, 3186–3196.

Zhou, Y. 1993 Degrees of locality of energy transfer in the inertial range. *Phys. Fluids* A **5**, 1092–1094.

Zhou, Y. & Vahala, G. 1993 Reformulation of recursive renormalization-group based subgrid modeling of turbulence. *Phys. Rev.* E **47**, 2503.

https://doi.org/10.1017/S0022112099007582 Published online by Cambridge University Press